Scientific report
WR 95-02

Ministerie van Verkeer en Waterstaat
Koninklijk Nederlands
Meteorologisch Instituut

Internal variability of the ocean generated by a stochastic forcing

M.B.H. van Noordenburg

De Bilt, 1995

KNMI

Scientific report; WR 95-02

De Bilt 1995

Postbus 201
3730 AE De Bilt
Wilhelminalaan 10
Telefoon 030-206 911
Telefax 030-210 407

Afstudeerverslag TU Delft

UDC: 551.461
519.216

ISSN: 0169-1651

ISBN: 90-369-2068-X

Internal Variability of the Ocean Generated by a Stochastic Forcing

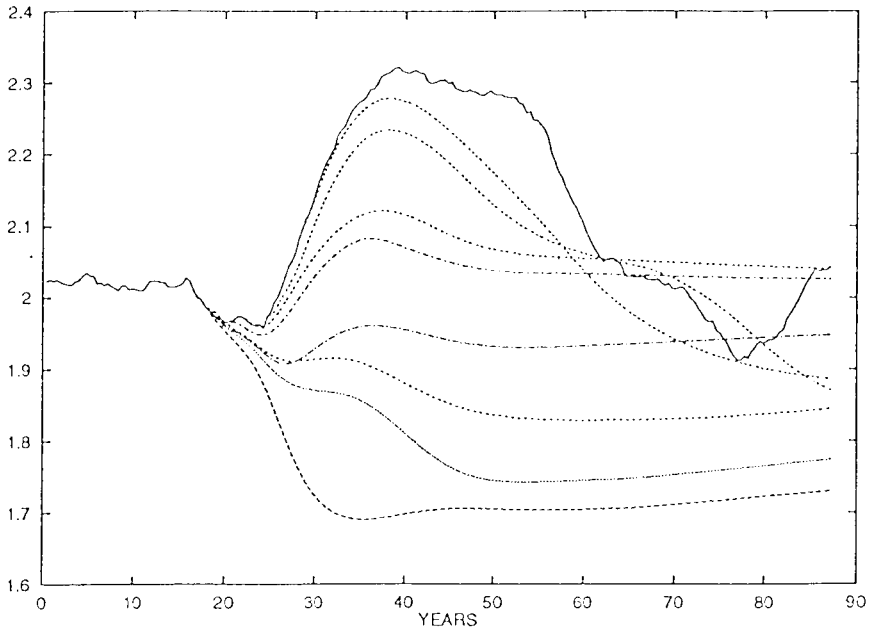

Afstudeerverslag

M.B.H. van Noordenburg

KNMI, January 1995

Abstract

In this study we investigate the internal variability of the ocean circulation under a stochastic perturbation of the freshwater flux. The ocean model we use in this study is a simple geostrophic model, which consists of a perfectly isolated rectangular basin with twelve layers in the vertical. At the surface mixed boundary conditions are applied, i.e. a restoring condition for temperature and a prescribed freshwater flux. If a stochastic perturbation is added to the freshwater flux the behaviour of the system displays an oscillating character with a characteristic period in the order of 100 years.

Analysis of the dynamical behaviour of the system indicates that besides stable also unstable equilibria are important for the time evolution of the model. The most important physical process for the variability in the thermohaline circulation is the process of deep water formation. This process appears to be sensitive to perturbations of the freshwater. At decadal time scales the freshwater flux strongly determines the variations in the process of deep water formation. On longer time scales the internal dynamics of the ocean model becomes more important. This rather strong influence of small perturbations of the freshwater emphasize the need for a more careful description of the hydrological cycle in the ocean-atmosphere system.

The characteristic time scale of about 100 years appears to be related to diffusive processes controlling temperature variations in the deep ocean. A more detailed study to investigate the temperature variations in the deep ocean is however necessary.

Contents

Chapter 1

Introduction

During the last decades there is a growing interest in the possible influence of human activity on climate change. Especially the issue of "global warming" has received much attention. The climate system however contains a substantial amount of natural variability. Therefore it remains unclear, whether changes in the climate, past or future, are due to human activities or to this natural variability. Our knowledge about this natural variability on decadal or longer time scales is rather poor. Almost all instrumental records are generally shorter than 100 years and not so accurate as one would like them to be. So the major difficulty on this time scale range is the insufficient data base. In order to try to understand however the basic physics of this natural variability a lot of research using computer models has been done.(see [9], [10], [11], [12], [13], [19] and [20])

The climate system can roughly be divided into two components, i.e. the atmosphere and the ocean. These two components can of course not be considered as two completely separated systems. The ocean and atmosphere are coupled and several feedback mechanisms exist between them. On a short time scale of about a few days the influence of the the ocean onto the atmosphere can be considered to be constant. Thereby making the use of constant sea surface temperatures (SST) in weather prediction models possible. On longer time scales however the feedback mechanisms between the ocean and the atmosphere become important. Climate models therefore must contain an atmospheric as well as an oceanic component. State of the art climate models require large computer resources making long runs over hundreds or thousands of years, which are needed for climate simulations, very expensive. At present only a small number of climate integrations in

the order of 1000 years has been performed at a few research centers in the world. Apart from the enormous computer resources required the problems in analyzing the results of these experiments are also tremendous. Therefore a hierarchy of climate models has been developed ranging from state of the art climate models to energy balance models in which the dynamics of the ocean and the atmosphere are reduced to simple diffusive processes.

The ocean is characterized by large heat capacity and large characteristic time scales, therefore it is assumed that a large part of the internal variability of the climate system on decadal and centennial time scales can be attributed to the internal variability of the ocean. In order to investigate the natural variability of the ocean simple models, which only contain an oceanic component, have been developed. The ocean circulation is driven by wind forcing and density differences. The atmosphere generates density differences in the ocean by the exchange of heat and freshwater, which affect respectively the heat and salinity distributions in the ocean. In ocean models this is parameterized by prescribing boundary conditions.

The heat exchange between the ocean and atmosphere is usually prescribed by linear relaxation of the sea surface temperature to a prescribed temperature distribution. This prescribed temperature distribution is often assumed to be constant in time and only spatial variations are taken into account. The magnitude of the ocean-atmospheric heat exchange is then determined by the difference between this temperature distribution and the sea surface temperature. The freshwater flux, precipitation minus evaporation, is usually assumed to be constant in time and independent of the state of the ocean. The atmospheric forcing onto the ocean is however continuously varying. Apart from the seasonal cycle the ocean and atmosphere are interacting with each other on small space and time scales. Several Studies (see [5], [14], [17] and [18]), have shown, that the behaviour of an ocean model is very sensitive to small perturbations in the freshwater flux.

In certain polar areas the surface waters are so strongly cooled that they sink to the bottom of the ocean. This process of deep water formation affects the density distribution in the ocean and generates among others warm currents like the Gulf Stream to which Europe owes its mild climate. The deep water formation can however easily be interrupted by an additional freshwater flux which makes the surface waters less dense. Likewise deep water formation can be triggered by a smaller than normal freshwater flux.

To account for the time dependence of the freshwater flux, at least qualitatively, a stochastic component will be added. It is hoped that in first order this stochastic forcing describes the effect of the high frequency mid-

latitude cyclones, which have a characteristic time scale in the order of 5 days. Whether this represents a more realistic description of the freshwater flux is could be questioned. For instance the effect of the sea surface temperature distribution on the location and intensity of the midlatitude cyclones is not taken into account. It is however hoped that the inclusion of a stochastic forcing will increase the understanding of the oceanic component and that this will also be relevant for understanding the coupled ocean-atmosphere system. In this report the effect of this stochastic perturbation on the natural variability of the ocean circulation will be studied. Especially the physical principles, which are important for this variability will be investigated in detail.

In chapter 2 a simple stochastic theory is used to investigate the theoretical influence of the atmosphere onto the ocean circulation. The ocean model, which will be used in this investigation is described in chapter 3. All boundary conditions are defined and the stochastic component of the freshwater flux is introduced. In chapter 4 an attempt is made to give a phase space description of the natural variability generated by this model. The physical processes, which are important for this variability are investigated in detail in chapter 5. In chapter 6 the main conclusions are summarized.

Chapter 2

Stochastic climate models

In order to investigate the influence of the atmosphere onto the ocean circulation a theory about simple stochastic climate models is considered. For this purpose the total climate system is divided into a rapidly varying "weather" system and a slowly responding "climate" system. The influence of the "weather" components onto the "climate" system is described through random forcing terms. Whereas the climate variability can be considered to be the integrated signal of these short period excitations.

2.1 Introduction

In the theory about stochastic climate models as described in Hasselmann [2] a few basic assumptions are made. First we assume, that we have a set of equations, which completely describes the evolution of the whole system, i.e. that we have a set of equations, which describes the large scale processes, such as the thermohaline circulation, sea surface temperature (SST), as well as the small scale processes, such as cloudiness, rainfall, etc. , on all time scales exactly.

The equation governing the evolution of the system is given by

$$\frac{dz_i}{dt} = w_i(z), \tag{2.1}$$

where w is, in general, a complicated nonlinear function of z.

The second assumption is that we can divide the total system into two subsystems, i.e.

$$\frac{dx_i}{dt} = u_i(x, y) \tag{2.2}$$

$$\frac{dy_i}{dt} = v_i(x, y) \tag{2.3}$$

$$\text{with} \quad O(x_i(\frac{dx_i}{dt})^{-1}) = \tau_x \ll \tau_y = O(y_i(\frac{dy_i}{dt})^{-1}). \tag{2.4}$$

The constant τ_x (τ_y) is an estimate of the time scale of the phenomena associated with the variable x (y).

Changes in the atmosphere usually take place on short time scales of about a few days, in contrast to changes in the ocean, which act on time scales of months, years, decades or even longer. In general condition (2.4) will thus be fulfilled.

Most of the derivations are omitted in this paragraph and are given in Appendix A.

2.1.1 Linear case, $\tau_x \ll t \ll \tau_y$

We first assume that $\tau_x \ll$ t $\ll \tau_y$, which implies that we are able to neglect the influence of feedback mechanisms. From now on it will be assumed that ergodicity holds, so that ensemble averaging and time averaging are equivalent.

If we start from an initial climate state y_0, the relative change of the actual climate state $y(t)$ to y_0 is given by δy = $y(t)$ - y_0. This relative change can be divided into a mean and a fluctuating term, i.e.

$$\delta y = \langle \delta y \rangle + \delta y', \tag{2.5}$$

where $\langle \ldots \rangle$ denotes the ensemble average over the variable x.

This decomposition is known as the Reynolds decomposition (see [15]). We here consider the case that $t \ll \tau_y$, which makes it possible to regard y as a constant in the forcing term on the right hand side of (2.3). By substituting the Reynolds decomposition in (2.3) and taking the ensemble average, we get

$$\frac{d\langle \delta y_i \rangle}{dt} = \langle v_i(x, y_0) \rangle. \tag{2.6}$$

By subtracting this equation from (2.3) we obtain a differential equation for the fluctuating term, i.e.

$$\frac{d\delta y_i'}{dt} = v_i(x, y_0) - \langle v_i \rangle = v_i', \tag{2.7}$$

where $\langle v_i' \rangle = 0$ and $\delta y_i' = 0$ for t=0.

The statistics of $v_i'(t)$ are defined through the statistics of the weather variables x(t), because we take the ensemble average over x for fixed y_0. It is assumed that x(t), and therefore v'(t), represents a stationary random process[1].

The cross spectrum, $F_{ij}(\omega)$, of $v_i'(t)$ is defined as

$$F_{ij}(\omega) \;=\; \langle V_i(\omega) V_j^*(\omega) \rangle, \tag{2.8}$$

where $V_i(\omega)$ denotes the Fourier transform of $v_i'(t)$ and $*$ the complex conjugate. $v'(t)$ represents a stationary process and therefore the cross spectrum is equivalent to

$$F_{ij}(\omega) \;=\; \frac{1}{2\pi} \int_{-\infty}^{\infty} P_{ij}(\tau) e^{-i\omega\tau} d\tau, \tag{2.9}$$

with $P_{ij}(\tau) \;=\; \langle v_i'(t+\tau) v_j'(t) \rangle$.

By solving equation (2.7) in the Fourier domain we are able to calculate the cross spectrum of $\delta y_i'(t)$, $G_{ij}(\omega)$, yielding

$$G_{ij}(\omega) \;=\; \frac{F_{ij}(\omega)}{\omega^2} \qquad (\omega \neq 0). \tag{2.10}$$

In reality there exists a cut-off time lag $O(\tau_x)$ such that $P_{ij}(\tau) \approx 0 \; for \; \tau > \tau_x$, which means that for frequencies $\omega \ll \tau_x^{-1}$ the exponential in (2.9) can be set to one, so that $F_{ij}(\omega) \approx F_{ij}(0)$. We can therefore replace equation 2.10 by

$$G_{ij}(\omega) \;=\; \frac{F_{ij}(0)}{\omega^2} \qquad (\tau_y^{-1} \ll \omega \ll \tau_x^{-1}) \tag{2.11}$$

In most climate applications the response will lie in the low frequency range $\omega \ll \tau_x^{-1}$, where the input can be regarded as white and equation (2.11) is applicable. We find thus here that white noise results in a red response spectrum.

From (2.7) we can also obtain the deviation covariance of $\delta y'$

$$\langle \delta y_i' \delta y_j' \rangle \;=\; 2\pi t F_{ij}(0). \tag{2.12}$$

This relationship is called the dispersion relationship and has also been found by Hinze [3]. The covariance grows linear in time, which means that the covariance becomes very large as t becomes very large. This is of course not very realistic, because this would mean that ice-age amplitudes could occur within time periods in the order of a century, which is clearly in contradiction with reality.

[1] stationary means that the probability density distribution is independent of time

2.1.2 Linear feedback, t = O(τ_y)

The above found equations can therefore only be valid if t $\ll \tau_y$ and in climate studies one is usually interested in longer time scales. So far we neglected the influence of feedback mechanisms, which are present in the climate system and if we want to look at times, which are O(τ_y), we have to take them into account. We therefore need a new set of equations to describe the evolution of the system. The variable y represents a random variable and therefore a differential equation for the probability density distribution, $p(y,t)$, of the climatic states y should be derived. This differential equation can be obtained by expanding the so-called Master equation (see [7]). To construct an analytical solution for an arbitrary nonlinear climate model will however normally not be possible.

For the special case of small excursions of the climatic states around an stable equilibrium state y=0 the solution can be derived analytically. In this case the evolution of the system can then be described by a so-called Langevin equation,

$$\begin{aligned} \frac{dy_i}{dt} &= V_{ij}y_j + v_i' \\ \text{with } y(t) &= y_0 \text{ at } t = 0. \end{aligned} \tag{2.13}$$

The matrix V_{ij} must be negative definite, because of the assumption that we have a stable equilibrium point.

It can be shown that in this case the Langevin equation is equivalent to the Fokker-Planck equation (see [7]). Like before we want to know the cross spectrum and this time we take the cross spectrum of y(t), because we have a system with fluctuations around a stable equilibrium y=0. If we, for simplicity reasons, assume that V is a diagonal matrix with λ_i on the diagonal, we get for the cross spectrum

$$G_{ij}(\omega) = \frac{F_{ij}(0)}{(\omega + i\lambda_i)(\omega - i\lambda_j)}. \tag{2.14}$$

If we compare this to (2.11) we see that for large ω the behavior is identically to that in the linear case. This is logical, because for large ω it holds that $t \ll \tau_y$. For small ω, thus $t = O(\tau_y)$, we find that the cross spectrum remains bounded.

The deviation covariance, which is now defined as $[y_i'y_j'] = [(y_i - y_{i0})(y_j - y_{j0})]$, also remains bounded, which is in accordance with expectations.

$[\ldots]$ denotes the ensemble average over the variable y.

Chapter 3

Model description

The theoretical approach, which was followed in the previous chapter, predicted that the natural variability of the ocean takes place on all possible time scales. In the remainder of this investigation a simple ocean general circulation model will be used to test, whether this kind of variability can also be established numerically. The model contains only a oceanic component and the influence of the atmosphere onto the ocean is described through boundary conditions, thereby neglecting the several feedback mechanisms, which are present in the real climate system. The wind stress is prescribed and assumed to be constant in time, whereas the heat exchange between ocean and atmosphere is parameterized by linear relaxation. The freshwater flux is also prescribed and assumed to be constant in time. The ocean and atmosphere are however continuously interacting and so the atmospheric forcing onto the ocean is never steady. As a first approximation of the time dependence of the atmospheric forcing a stochastic component is added to the freshwater flux.

3.1 Introduction of the model

The model is a 3-dimensional geostrophic model, which was developed by Lenderink and Haarsma and is described in Lenderink [9]. Here only the main characteristics of the model are described. For details the reader is referred to Lenderink [9]. The model consists of a rectangular basin with longitudinal extension L and latitudinal extension M, in which the curvature of the earth and the bottom topography of the ocean are absent. This idealized ocean is centered around 45° N and consists of 12 layers in the ver-

tical with varying thickness. In each layer the temperature (T), salinity (S) and velocity distributions are allowed to vary continuously in the horizontal, but are assumed to be independent of the depth. In addition geostrophy is assumed, which implies a balance between the coriolis force and pressure gradient force. By assuming geostrophy the fast modes of the ocean, such as Kelvin waves, are filtered out. On a climatic time scale these fast waves are assumed to be unimportant. The windstress acts on the surface. At the surface a rigid lid approximation is made, which means that surface displacements are neglected in the continuity equation. The model is relatively simple, but gives fairly realistic solutions. It can easily be used for long term integrations.

3.2 The model equations

The model equations are the Navier-Stokes equations along with the conservation equations for heat, salinity and mass and an equation of state (see Appendix B). In first order sea-water is incompressible and so the density, ρ, can be taken constant in the continuity-equation, yielding

$$\nabla_3 \cdot \vec{u} \;=\; 0. \tag{3.1}$$

Using the assumption that the velocity distribution in a layer is independent of the depth we can integrate over the depth of a layer, which gives

$$w_1 \;=\; h_1 \nabla_2 \cdot \vec{u}_1 \tag{3.2}$$

$$w_i \;=\; h_i \nabla_2 \cdot \vec{u}_i \;+\; w_{i-1} \qquad i = 2, \ldots, 11 \tag{3.3}$$

$$-w_{11} \;=\; h_{12} \nabla_2 \cdot \vec{u}_2, \tag{3.4}$$

where w_i is the vertical velocity from layer i+1 to layer i.

In this model the depth of the basin is taken to be much smaller than the longitudinal and latitudinal extension of the basin. From scaling arguments it follows that w $\ll$ u,v. For the vertical momentum equation therefore hydrostatic equilibrium is assumed, which implies a balance between the vertical pressure gradient force and the gravity force (see [4]),

$$\frac{\partial p}{\partial z} \;=\; -\rho g \tag{3.5}$$

Away from the boundaries geostrophy is assumed for the horizontal momentum equations, which means that the term D$\vec{u}$/Dt is neglected. This

is a good approximation if the Rossby number, $R \equiv U/f_0 L \ll 1$. Here L is a spatial scale on which the velocity varies, U is a characteristic scaling velocity and f_0 is the Coriolis parameter. A typical velocity of the ocean is 10 cm/s and $L = 10^5$m which yields $R \approx 10^{-2}$ and the approximation is thus justifiable. Again using the assumption, that the velocity distributions are independent of the depth of a layer we can integrate the horizontal momentum equations over the depth of a layer and get

$$\begin{aligned}
fu_1 &= -\frac{1}{\rho_0}\frac{\partial p_1}{\partial y} - \kappa_s v_1 + \frac{\tau_y}{h_1\rho_0} \\
fu_i &= -\frac{1}{\rho_0}\frac{\partial p_i}{\partial y} - \kappa_s v_i \qquad i = 2,\ldots,12 \\
-fv_1 &= -\frac{1}{\rho_0}\frac{\partial p_1}{\partial y} + \frac{\tau_x}{h_1\rho_0} \\
-fv_i &= -\frac{1}{\rho_0}\frac{\partial p_i}{\partial y} \qquad i = 2,\ldots,12,
\end{aligned} \tag{3.6}$$

where f is the coriolis force and τ is the windstress. Here the assumption is made that the depth of the Ekman spiral is less than the depth of the first layer. For the coriolis force the β-plane approximation is used (see [4])

$$f(y) = f_0 + \beta y, \tag{3.7}$$

where $f_0 = 10^{-4}\mathrm{s}^{-1}$ and $\beta = 2.10^{-11}\mathrm{m}^{-1}\mathrm{s}^{-1}$, which are the approximate values at 45°N and y is the poleward distance. In the momentum equation for v a linear friction term, which is called the Stommel-friction, is included to generate a boundary current, which closes the circulation. The parameter κ_s determines the strength of the friction. Friction between layers and molecular viscosity are neglected.

Integration of the equation of conservation of salinity over the depth of a layer gives

$$\begin{aligned}
&\frac{\partial S_1}{\partial t} + \nabla_2\cdot(\vec{u}_1 S_1) - w_1 S_1^\star/h_1 = \kappa_h\nabla_2^2 S_1 + \Phi_v^{S_1} + \Phi_a^{S_1} \\
&\frac{\partial S_i}{\partial t} + \nabla_2\cdot(\vec{u}_i S_i) + (w_{i-1}S_{i-1}^\star - w_i S_i^\star)/h_i = \kappa_h\nabla_2^2 S_i + \Phi_v^{S_i} \\
&\qquad\qquad i = 2,\ldots,11 \\
&\frac{\partial S_{12}}{\partial t} + \nabla_2\cdot(\vec{u}_{12}S_{12}) + w_{11}S_{11}^\star/h_{12} = \kappa_h\nabla_2^2 S_{12} + \Phi_v^{S_{12}},
\end{aligned} \tag{3.8}$$

where κ_h is a horizontal diffusion coefficient, $\Phi_v^{S_i}$ symbolizes the effect of vertical diffusion and convection and $\Phi_a^{S_1}$ represents the salinity forcing of

the atmosphere. Convection occurs when the vertical stratification of the layers is unstable. $S_1^\star$ is defined as

$$S_1^\star = \begin{cases} S_1 & \text{if } w_1 < 0 \\ S_2 & \text{if } w_1 > 0. \end{cases}$$

This can be considered as an upwind differencing scheme. The other variables with a star are equally defined. The derivation of the heat equations is equivalent to that of the salinity equations

$$\begin{aligned}
&\frac{\partial T_1}{\partial t} + \nabla_2 \cdot (\vec{u}_1 T_1) \quad - \quad w_1 T_1^\star / h_1 \quad = \quad \kappa_h \nabla_2^2 T_1 + \Phi_v^{T_1} + \Phi_a^{T_1} \\
&\frac{\partial T_i}{\partial t} + \nabla_2 \cdot (\vec{u}_i T_i) + (w_{i-1} T_{i-1}^\star - w_i T_i^\star)/h_i \quad = \quad \kappa_h \nabla_2^2 T_i + \Phi_v^{T_i} \\
&\qquad\qquad\qquad\qquad\qquad\qquad\qquad\qquad\qquad\qquad\qquad\qquad\qquad\qquad i = 2, \ldots, 11 \\
&\frac{\partial T_{12}}{\partial t} + \nabla_2 \cdot (\vec{u}_{12} T_{12}) \quad + \quad w_{11} T_{11}^\star / h_{12} \quad = \quad \kappa_h \nabla_2^2 T_{12} + \Phi_v^{T_{12}}, \quad (3.9)
\end{aligned}$$

where again $\Phi_v^{T_i}$ symbolizes the effect of vertical diffusion and $\Phi_a^{T_1}$ represents the atmospheric forcing. The variables with a star are determined in the same way as for salinity.

The equation of state is approximated by

$$\rho = \rho_0 + \alpha_S S + \alpha_T (T - T^\star)^2, \tag{3.10}$$

with $\alpha_S = 0.7739\ kg\ m^{-3}$ per promille, $\alpha_T = 0.00471\ kg\ m^{-3} K^{-2}$, $T^\star = 265.42$ K and $\rho_0 = 1001.3263\ kg\ m^{-3}$. The units of T and S are Kelvin and PSU(promille) respectively. In this approximation we assume, that the density of sea-water is independent of the pressure.

3.2.1 Boundary conditions

The velocities normal to the boundaries are zero

$$\vec{u} \cdot \vec{n} = 0, \tag{3.11}$$

where $\vec{n}$ is the normal vector at the boundary. The no-slip condition is not imposed, which means that the velocity tangential to the boundary need not to be zero. We also assume that we have a perfectly isolated basin without any gain or loss of heat and salt across the boundary, i.e.

$$\nabla_2 S \cdot \vec{n} = \nabla_2 T \cdot \vec{n} = 0. \tag{3.12}$$

3.2.2 Values of parameters and forcing fields

The numerical implementation has been done by Lenderink and Haarsma and is described in Lenderink [9]. The description of the numerical implementation will be omitted here and only some numerical values will be given. The dimensions of the basin are 5000 by 5000 km with a grid point distance of 250 km. The total depth is 4000 m and the basin is divided into 12 layers with thickness;

$h_1 = 30$, $h_2 = 50$, $h_3 = 80$, $h_4 = 140$, $h_5 = 250$, $h_6 = 350$,

$h_7 = 400$, $h_8 = 450$, $h_9 = 500$, $h_{10} = 550$ and $h_{11} = h_{12} = 600$ m.

The time step used in the experiments is 5 days, but for stability reasons this time step is sometimes reduced to 2.5 days. The atmospheric forcing term in equation 3.8 is determined by the precipitation minus evaporation (P-E) rate. It can be transformed into a salt flux, by using the salt conservation law for a layer with initial thickness h_1, salinity S_1 and a freshwater flux x_{P-E}, giving

$$h_1 S_1 = (h_1 + x_{P-E}\delta t)(S_1 + \delta S). \tag{3.13}$$

In first order this yields

$$\frac{\partial S_1}{\partial t} = -\frac{S_1 x_{P-E}}{h_1} \approx -\frac{S^* x_{P-E}}{h_1}, \tag{3.14}$$

where S^* is the mean salinity of the layer. This salt flux can easily be included in equation 3.8. The freshwater flux and hence the salt flux is assumed to be independent of the state of the ocean. In the experiments the salt flux is constant in time and the spatial variation is of the form

$$\Phi_a^{S_1} = s_0 cos(\frac{\pi y}{M}). \tag{3.15}$$

This boundary condition represents net evaporation near the equator and net precipitation near the pole. For s_0 the value of $2.96 \cdot 10^{-8}$ PSU s^{-1} is chosen, which is equal to a maximum freshwater flux of 0.8 m/year. This is relatively weak compared to observations. An atmospheric forcing term also appears in the heat equations, but describing this term by a constant heat flux is not very realistic, because it would imply that heat anamolies could exist for a long period of time in the surface layer. A more appropriate way to describe this term is through relaxation towards an atmospheric temperature, making fast heat exchange between ocean and atmosphere possible, i.e.

$$\Phi_a^{T_1} = \alpha_\tau (T_{atm} - T_1). \tag{3.16}$$

The assumption is here, that the heat capacity of the atmosphere is unbounded. This is of course not very realistic. Nevertheless this boundary condition will be used in this investigation. The atmospheric temperature represents the idealized observed zonal averaged surface distributions and is of the form

$$T_{atm} = T_m(1 + cos(\frac{\pi y}{M})). \tag{3.17}$$

The constant α_T, which represents the time scale of the relaxation, is chosen to be 25 days and T_m is $28°C$, yielding a 28°C equator to pole difference. This is a fairly moderate difference. The influence of sea-ice is however neglected in the model, thereby making a larger difference impossible. The combination of relaxation towards an atmospheric temperature and a prescribed freshwater flux is called mixed boundary conditions. In the heat as well as in the salinity equations the term Φ_v represents the effect of vertical diffusion and convection. In the numerical implementation the strength of the vertical diffusion is determined by the constant κ_v with value $1 \cdot 10^{-4}\ m^2 s^{-1}$. The windstress τ has only a zonal component and roughly represents the observed climatological mean meridional distribution of the zonal winds with westerlies in the midlatitudes and easterlies in the subtropics, i.e.

$$\tau_x = -\frac{\rho_0 f M}{2\pi} w_{s0} cos(\frac{2\pi y}{M}), \tag{3.18}$$

where w_{s0} is a constant with value $5 \cdot 10^{-7}$, which is equal to a surface wind maximum of about 10 ms^{-1}. The horizontal diffusion coefficient and the Stommel-friction coefficient, κ_h respectively κ_s, are $3 \cdot 10^3\ m^2 s^{-1}$ and $1 \cdot 10^{-6}\ s^{-1}$.

3.3 Some measuring tools

The ocean is a 3-dimensional system and to describe its evolution in time it is useful to have some 1-dimensional or 2-dimensional quantities, which represent characteristics of the system. In this report we will use:

1. *Meridional overturning function*
   The meridional overturning function is a stream function, which can be derived from the continuity equation using boundary condition (3.11), i.e.

$$\int_0^L (\frac{\partial u}{\partial x} + \frac{\partial v}{\partial y} + \frac{\partial w}{\partial z})dx = \int_0^L (\frac{\partial v}{\partial y} + \frac{\partial w}{\partial z})dx = 0.$$

We can now define the meridional overturning function Φ by

$$\Phi(y,z) \;=\; \int_{x=0}^{L}\int_{k=z}^{0} v dk dx \tag{3.19}$$

The minimum and the maximum of Φ are quantities, which are often used to describe the behavior of the oceanic system.

2. *Meridional heat transport (MHT)*
   The meridional heat transport is the zonal integrated heat transport from equator to pole. It is mathematically defined as:

$$MHT(y) \;=\; \int_{z=-h}^{0}\int_{x=0}^{L} v\cdot T\cdot c_v dx dz \tag{3.20}$$

   where c_v denotes the specific heat of water, which is $4.2\cdot 10^6\ JK^{-1}m^{-3}$. The meridional mass, salt and volume transport are defined equivalently.

3. *Surface averaged heat flux (SHF)*
   The surface averaged heat flux is defined as:

$$SHF \;=\; \frac{1}{LM}\cdot\int_{x=0}^{L}\int_{y=0}^{M} c_v\cdot\alpha_\tau(T_{atm}-T_{surf})dxdy \tag{3.21}$$

Here L is the zonal and M the meridional extension of the ocean basin, c_v the specific heat of water and α_τ the relaxation time scale.

3.4 Spin-up

The spin-up experiment started from a homogeneous ocean with a temperature of $7°C$ and a salinity of 35.00 PSU (promille) and lasted for about 2000 years of integration, which is long enough to reach an equilibrium state. This equilibrium state is shown in figure 3.1. In the upper part of the ocean the velocity field (fig 3.1a) displays a clockwise gyre with a strong northward flow along the western boundary and a somewhat weaker reversed flow in the eastern region. At greater depth water is slowly flowing southwards along the western boundary. The temperature distribution (fig 3.1b) of the top layer of the basin is much alike the distribution of the atmospheric temperature due to the strong relaxation towards the atmospheric temperature. At

A

Velocity level 1

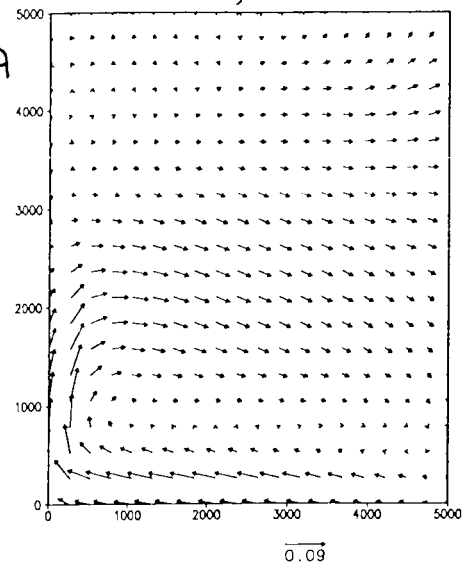

Velocity level 2

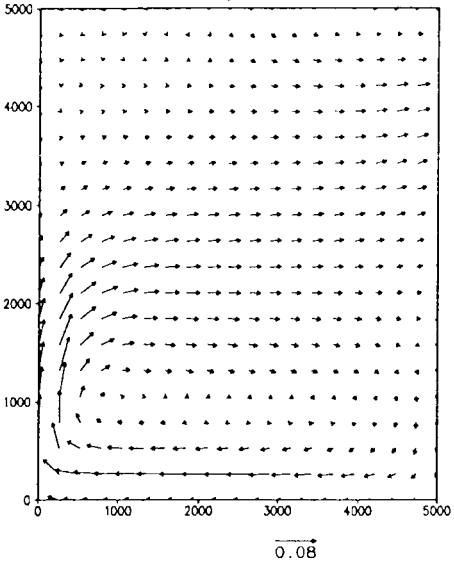

Velocity level 3

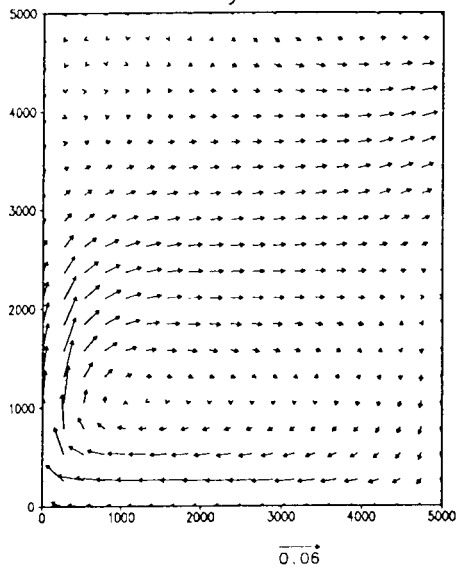

Velocity level 5

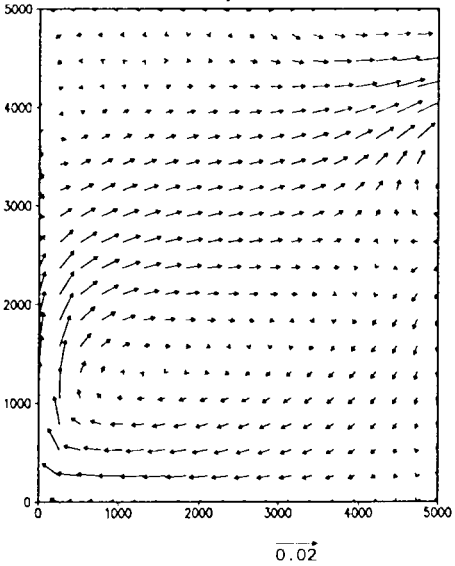

Velocity level 9

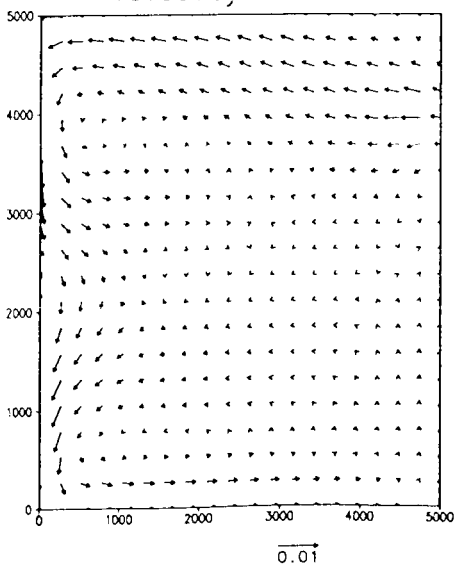

Velocity level 12

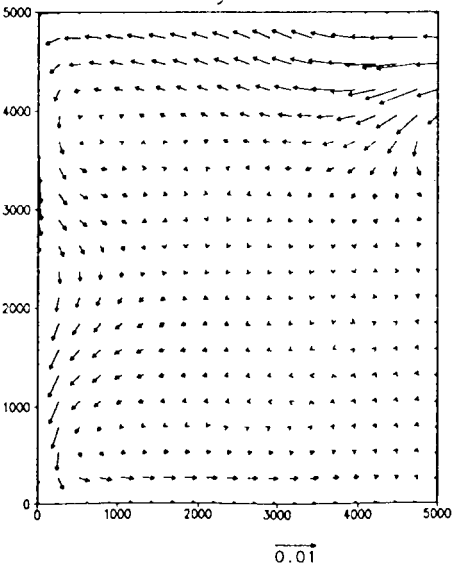

B

Temperature level 1

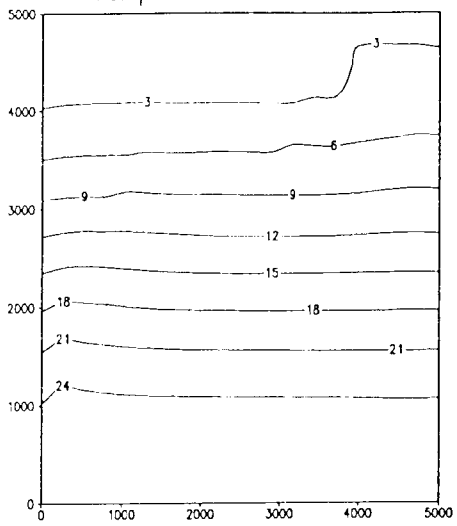

Temperature level 2

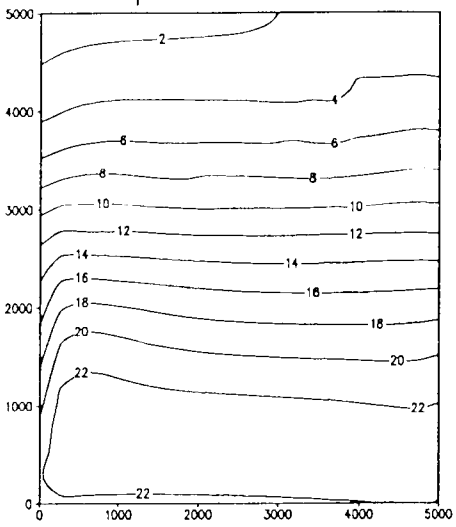

Temperature level 3

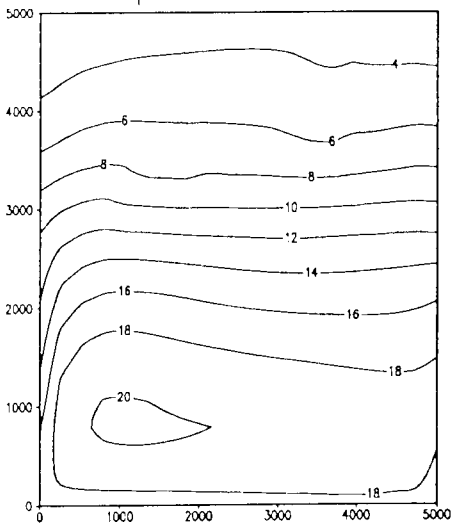

Temperature level 5

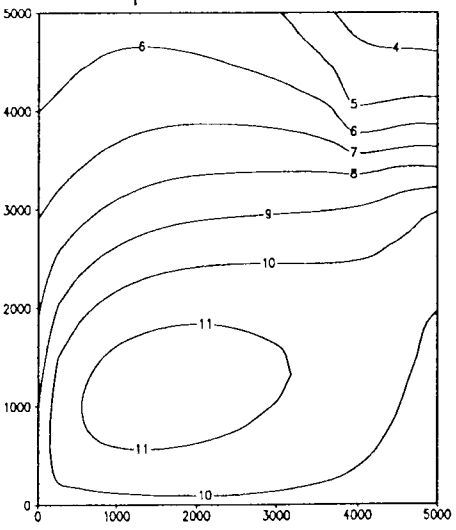

Temperature level 9

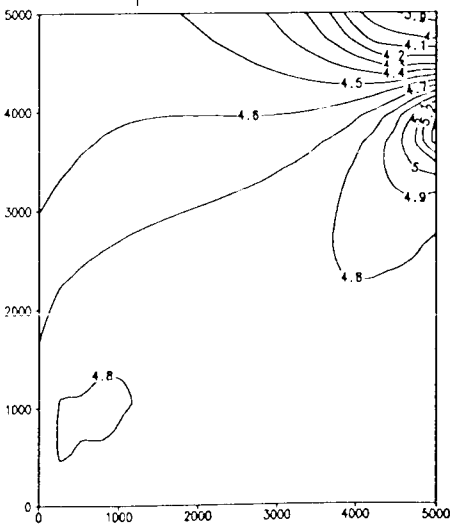

Temperature level 12

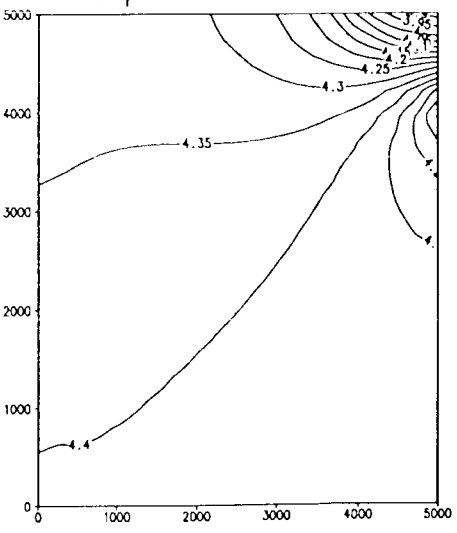

C

Salinity level 1

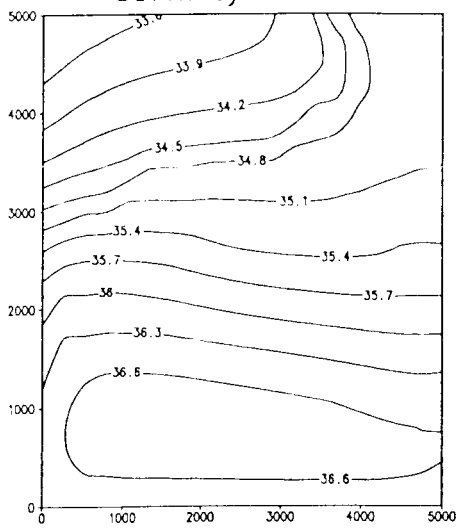

Salinity level 2

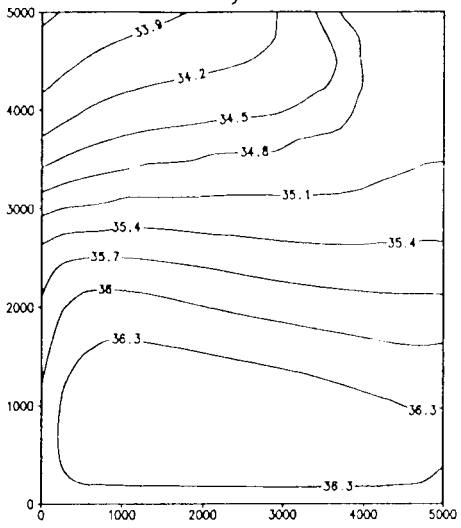

Salinity level 3

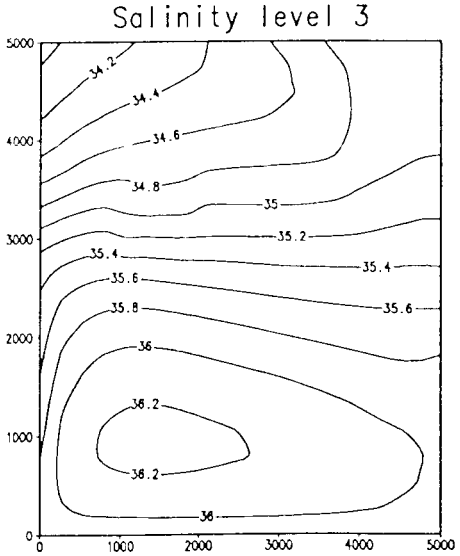

Salinity level 5

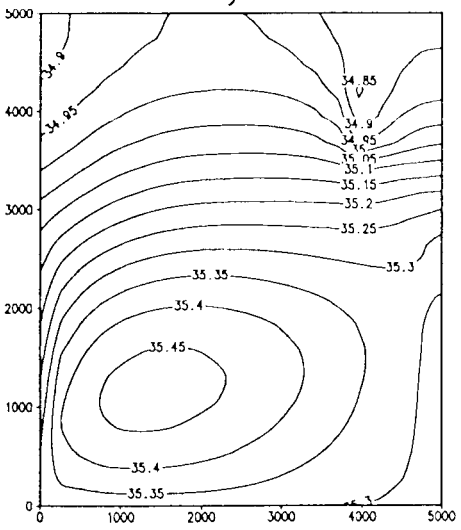

Salinity level 9

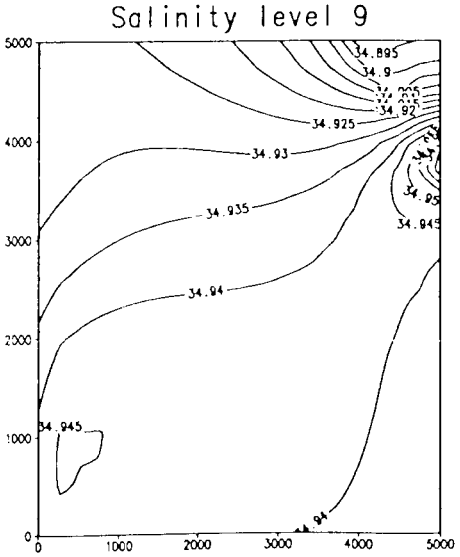

Salinity level 12

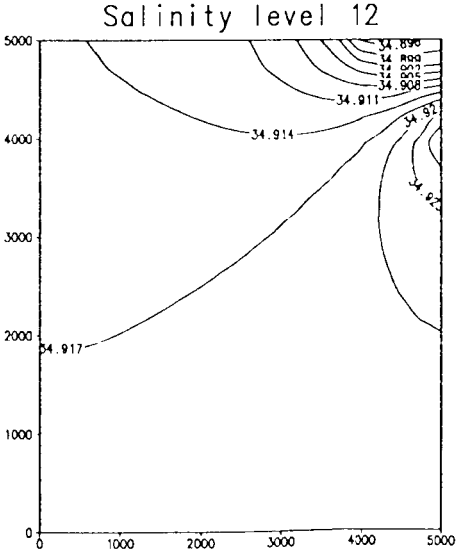

D

Verticalvelocity level 1

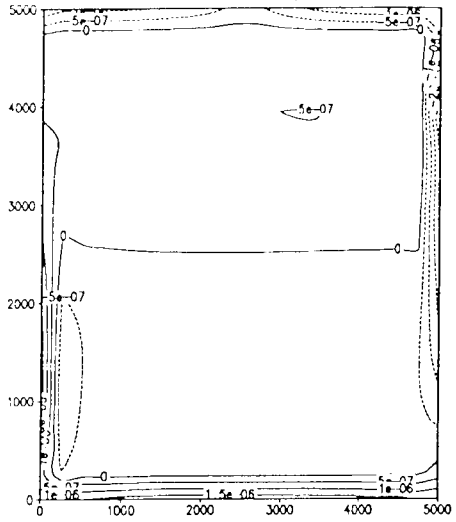

Verticalvelocity level 2

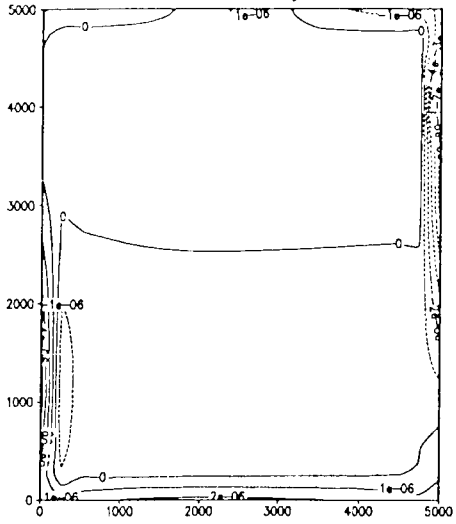

Verticalvelocity level 3

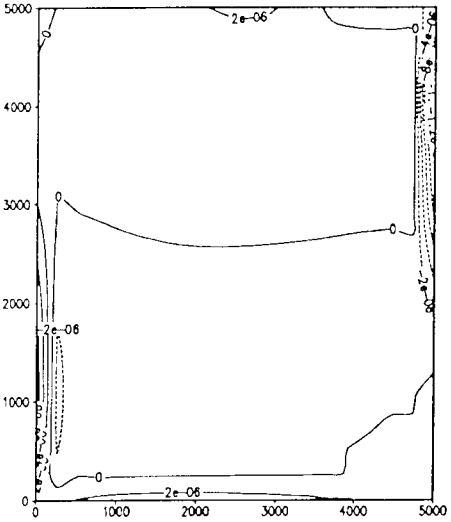

Verticalvelocity level 5

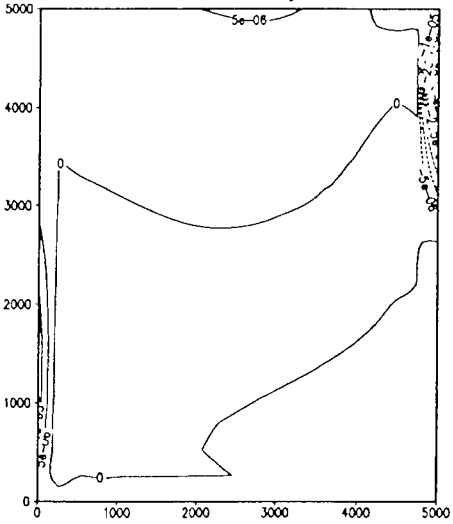

Verticalvelocity level 9

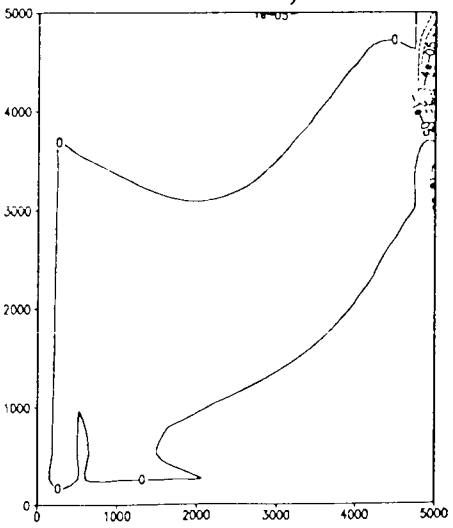

Verticalvelocity level 11

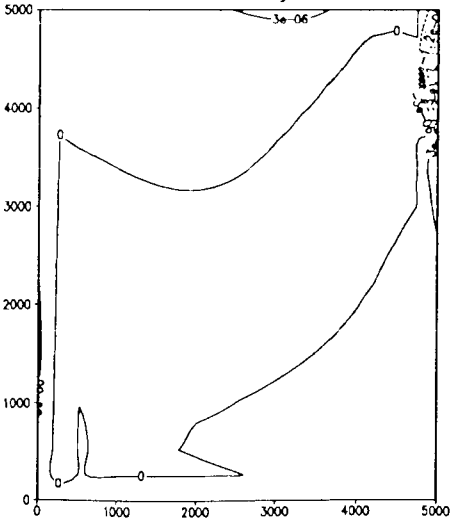

E

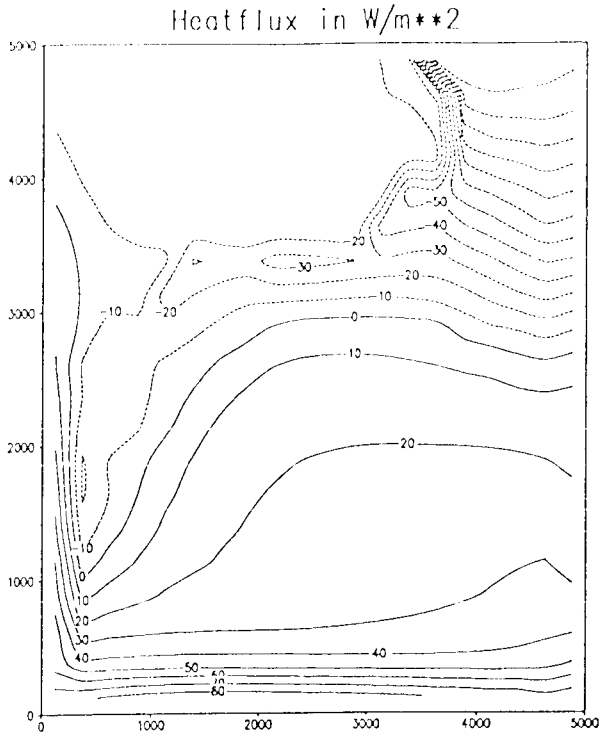

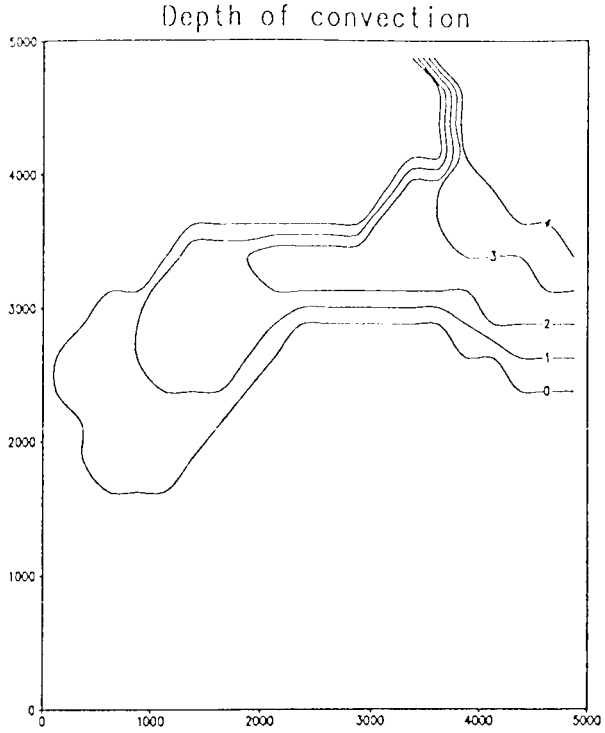

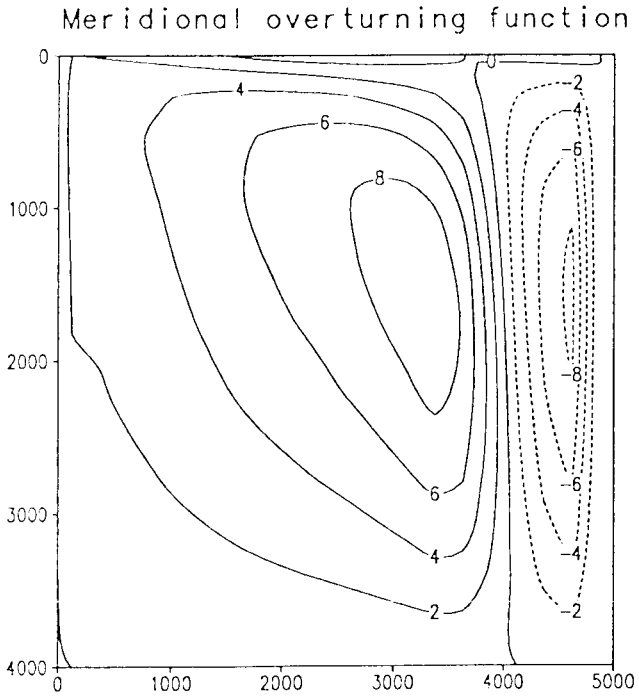

Figure 3.1: The spin-up state, figure a:velocity distribution in cm s^{-1}, figure b: temperature distribution in $^{\circ}C$, figure c: salinity distribution in PSU, figure d: vertical velocity distribution in cm s^{-1} and figure e: surface heat flux in Wm^{-2}, depth of convection in layers and meridional overturning function in Sverdrups.

deeper levels the temperature shows the gyre structure of the velocity field. This gyre structure is also perceptible in the salinity distribution (fig 3.1c). In contrast to the temperature the gyre is also present in the salinity distribution of the top layer.

One can further note that the western boundary region remains relatively cool and fresh due to the large vertical velocity (fig 3.1d), which transports cool and fresh deep oceanic water to the surface. We also see, that the vertical velocity is much smaller than the horizontal velocity. This is in accordance with our assumptions (see section 3.2). If we look at the surface heat flux (fig 3.1e), we see, that the ocean takes up a large amount of heat in the region near the equator and loses most of its heat in the convective area, which occurs in the northeastern part of the ocean. The effect of cooling near the poles is larger than the effect of precipitation, creating a relatively high surface density, which results in an unstable stratification. Deep oceanic water is then mixed to the surface resulting in a relatively warmer temperature and more saline salinity surface distribution in this region. This process is also taking place in the North Atlantic and is called the process of North Atlantic deep water (NADW) formation.

The most typical property of the meridional overturning function (fig 3.1e) is its two cell-structure with a fairly strong positive (clockwise) cell and a weaker and smaller negative (anticlockwise) cell. The large positive cell represents a zonal mean north-south circulation. At the surface the ocean is flowing northwards. Sinking of surface water (convection) occurs at the pole. At greater depth there is a southwards flow and rising occurs at the equator. This general zonal mean north-south circulation is often referred to as the "meridional overturning" of the ocean.

The sunradiance is the energy source on earth. This energy input is much larger at the equator than near the poles. This imbalance is compensated by a poleward energy transport. The atmosphere and the ocean each transport about half of the total energy. This energy transport of the ocean takes place through transport of heat by the meridional overturning. Warm water is flowing polewards along the surface and rapidly loses most of its heat to the atmosphere. At greater depth cooler water is flowing southwards. In our model the meridional heat transport is in the order of 10^{14} W, which is a factor 10 to weak in comparison to reality (see [16]). A possible reason is the fairly moderate 28°C atmospheric temperature difference from pole to equator, which is used in the model. This could also explain why the meridional overturning function is too weak . Nevertheless the circulation of the spin up state reasonably resembles the circulation in the North Atlantic

and is suitable for this kind of studies.

3.5 The stochastic component of the freshwater flux

The stochastic component of the freshwater flux is obtained by integrating a first-order Markovian process and is described in Weaver et al. [19]. The equation governing the evolution of the stochastic component of the forcing field F is given by

$$\frac{\partial F}{\partial t} = -\frac{F}{\tau_F} + \sqrt{\frac{2}{\tau_F}} S, \tag{3.22}$$

where $\Gamma = 2\pi\tau_F$ is the autocorrelation time scale of the process and S is a white noise process. Equation (3.22) determines the time evolution of F, but the spatial structure of S remains free.

By taking the Fourier transform of (3.22) we are able to calculate the spectrum (SP(ω)) of F. Fourier transformation gives

$$\hat{F}(\omega) = \frac{1}{i\omega + 1/\tau_F} \sqrt{\frac{2}{\tau_F}} \hat{S}(w)$$

and so yielding a spectrum of

$$SP(\omega) = < \hat{F}(\omega)\hat{F}^*(\omega) > = \frac{2\tau_F/\pi}{1 + (\omega\tau_F)^2} < S^2 >, \tag{3.23}$$

where $< \ldots >$ denotes ensemble averaging and $< S^2 >$ is the variance of the process S.

The structure of (3.23) is white for periods longer than τ_F and falls off as ω^{-2} for shorter periods. This implies, that we can use $< S^2 >$ as a measure for the strength of the stochastic component F.

The white noise process S is usually chosen to be a Gaussian process, which makes it possible to use the Ito calculus to approximate equation (3.22). For simplicity reasons we take S to be standard Gaussian, which can always be achieved by scaling if S is a Gaussian process. The approximation of (3.22) is made by using a trapezoidal differencing scheme

$$\frac{F_{n+1} - F_n}{\delta t} = -\frac{F_{n+1} + F_n}{2\tau_F} + \sqrt{\frac{2}{\tau_F}} S.$$

After rewriting we get

$$\begin{aligned} F_{n+1}(1+\frac{\delta t}{2\tau_F}) &= F_n(1-\frac{\delta t}{2\tau_F}) + \sqrt{\frac{2}{\tau_F}}S\delta t \\ &= F_n(1-\frac{\delta t}{2\tau_F}) + \sqrt{\frac{2}{\tau_F}}(\triangle S_n). \end{aligned} \tag{3.24}$$

Because we have assumed that S is standard Gaussian distributed, it follows that

$$\begin{aligned} \triangle S_n &- \text{independent identically distributed } \forall n \\ &- \text{N}(0,\delta t) \text{ distributed} \end{aligned}$$

We can write $\triangle S_n$ as $\sqrt{\delta t}\ W_n$ with

$$\begin{aligned} W_n &- \text{independent identically distributed } \forall n \\ &- \text{N}(0,1) \text{ distributed} \end{aligned}$$

Substituting this in (3.24) we finally get:

$$\begin{aligned} F_{n+1} &= R_n F_n + (1-R_n^2)^{1/2} W_n \qquad (3.25) \\ \text{with} \qquad R_n &= \frac{1-\delta t/(2\tau_F)}{1+\delta t/(2\tau_F)}. \end{aligned}$$

Because the stability criterion is $|R_n| \leq 1$, (3.25) is absolutely stable. In the ocean model relatively large time steps are used and it is thus possible to include the discretisation scheme (3.25) directly into the model.

The choice for the spatial structure of the stochastic component of the freshwater flux is not determined by equation (3.22) and is essentially free. In this investigation we impose, however, some additional restrictions:

1. *Conservation of salt*
   In the model the assumption is made that for every time step the total amount of salt in the ocean remains constant. The stochastic forcing term F represents a freshwater flux, which can be related to an equivalent salt flux and so the condition of conservation of salt requires, that the spatial averaged contribution of F is zero.

2. *Only large scale structures*
   The stochastic component of the freshwater flux should represent the

precipitation minus evaporation fields of the large scale (O(1000 km)) weather systems like cyclones and anticyclones. With these fields it is possible to perturb large areas in the ocean with the same kind of perturbation, i.e. there is additional precipitation or evaporation over a large area at the same time.

3. *Limited water storage capacity*
   The water storage capacity of the atmosphere is limited. This means that, if there is precipitation over a larger area, the total amount of precipitation is restricted to a maximum value. In our model this can be achieved by requiring that the term $\overline{F_{n+1}^2}$ remains constant in time. (bar refers to spatial averaging)

To meet those restrictions a non-Gaussian distribution is chosen for W_n, although this is not correct from a mathematical point of view. The term W_n is given by:

$$W_n = \sum_{\bar{\kappa}} \hat{S}(k) cos(\bar{\kappa} \cdot \bar{x} + \phi(k)) \tag{3.26}$$

with $\hat{S}$(k) a specified constant and $\phi(k)$ a random phase between 0 and 2π with wavenumber k = $\langle \bar{\kappa} \cdot \bar{\kappa} \rangle^{1/2}$.

In this investigation only two waves are taken into account, i.e. (κ_x,κ_y) = $(4\pi/\mathrm{L},0)$ and $(0,4\pi/\mathrm{M})$. The spatial structure of the stochastic component of the freshwater flux is given in figure 3.2. This spatial structure can be shifted around the ocean. To measure the strength of the stochastic component of the freshwater flux we use the spatial averaged variance.

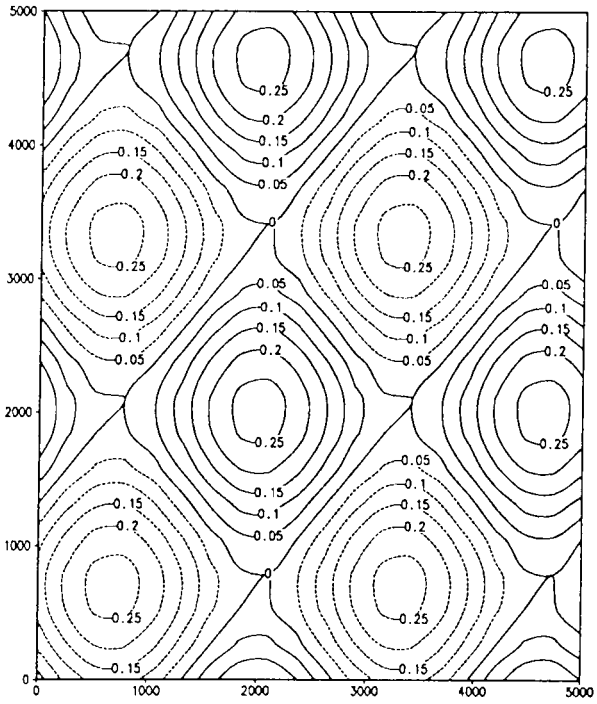

Figure 3.2: The stochastic perturbation of the freshwater flux in m/year.

3.6 Initial experiment

The spin-up state will from now on be used as starting point of our investigations and we will consider this as the origin of our time domain. To the standard deviation of the stochastic forcing, $< S^2 >^{1/2}$, a value of 0.4 times the maximum of the original freshwater flux is assigned, which is equivalent with 27 mm/month. We integrated the model for about 2500 years. The results are shown in figure 3.3 and 3.4.

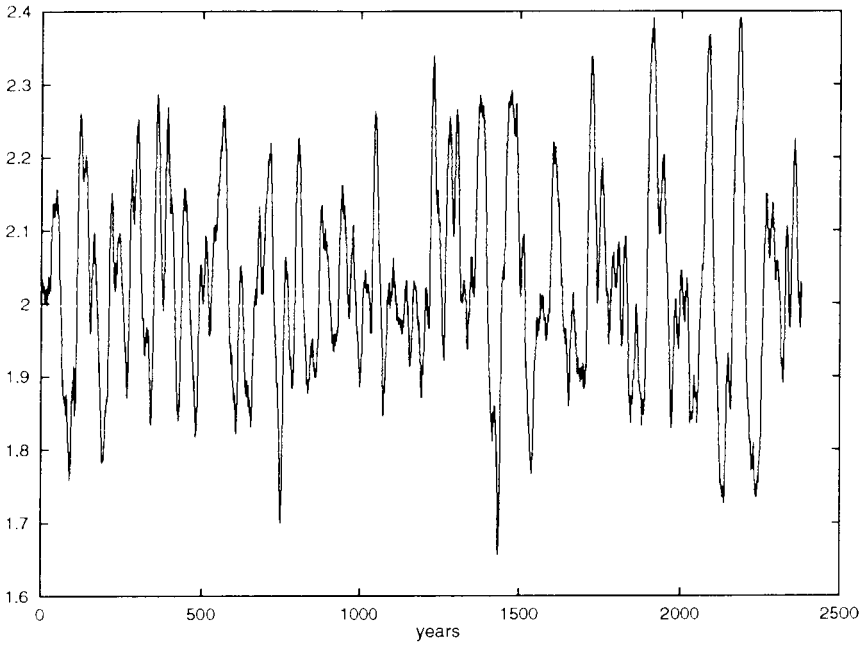

Figure 3.3: The meridional heat transport at y = M/2 in 10^{14} W under a stochastic forcing of 40 %.

The time series of the meridional heat transport (figure 3.3) shows a substantial variability with deviations from the equilibrium state in the order of 20 percent and an oscillating character. The time series of the maximum of the overturning function (figure 3.4a) and the meridional salt transport (figure 3.4b) strongly resembles that of the meridional heat transport. The time series of the temperature of the deep ocean (figure 3.4c) also displays similar variability. There is however a trend perceptible in the temperature of the deep ocean. During the first 1200 years the temperature increases. After 1200 years the temperature of the deep ocean drops substantially,

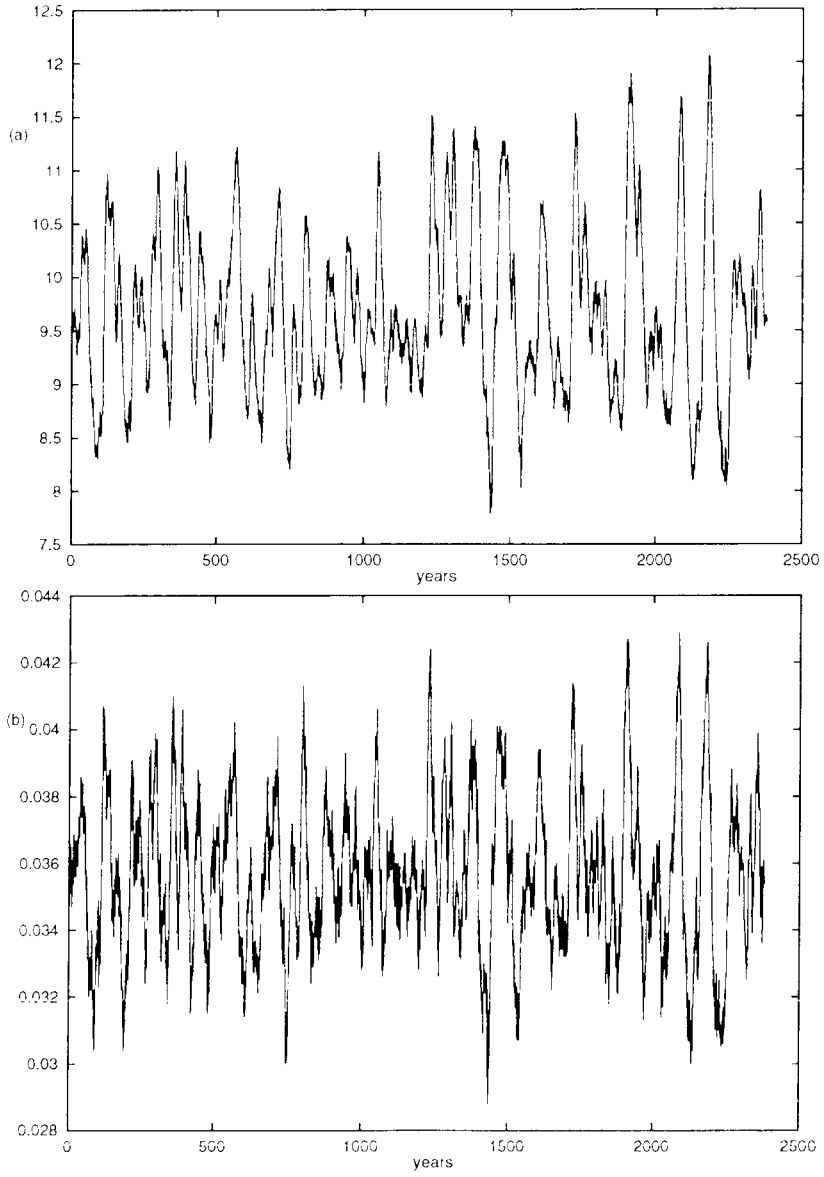
(a)
12.5
12
11.5
11
10.5
10
9.5
9
8.5
8
7.5
0
500
1000
1500
2000
2500
years
(b)
0.044
0.042
0.04
0.038
0.036
0.034
0.032
0.03
0.028
0
500
1000
1500
2000
2500
years

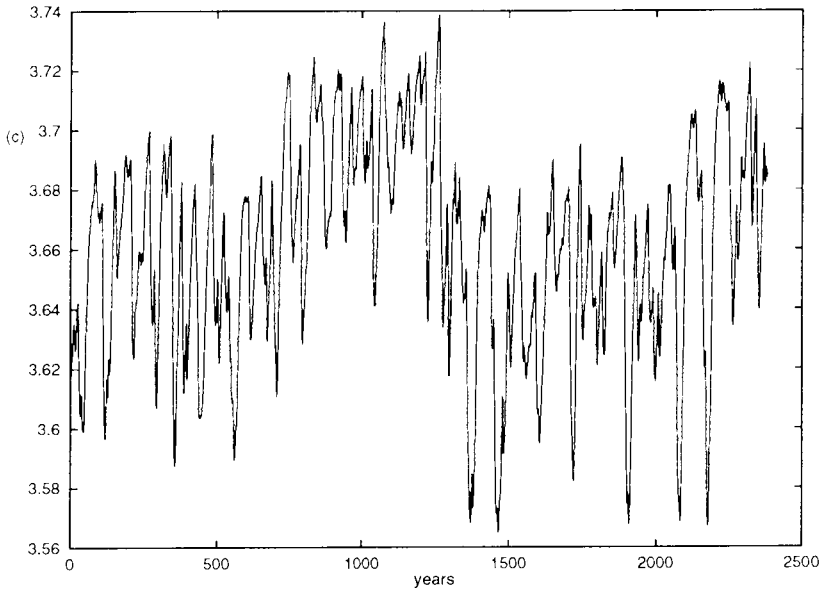

Figure 3.4: Time series of the several quantities a: maximum overturning in Sverdrups ($10^6 m^3 s^{-1}$), b: meridional salt transport in 10^8 PSU (promille) $m^3 s^{-1}$ at y=M/2, c: temperature of deepest layer of the ocean in °C, averaged over the top quarter of the basin.

hereafter the temperature of the deep ocean again tends to increase.

A closer inspection of the time series of the meridional heat transport suggests that there is a period of about hundred years in the variability. The variance spectrum of the time series shows indeed a peak around periods in the order of a century (See figure 3.5). This phenomenon is also perceptible

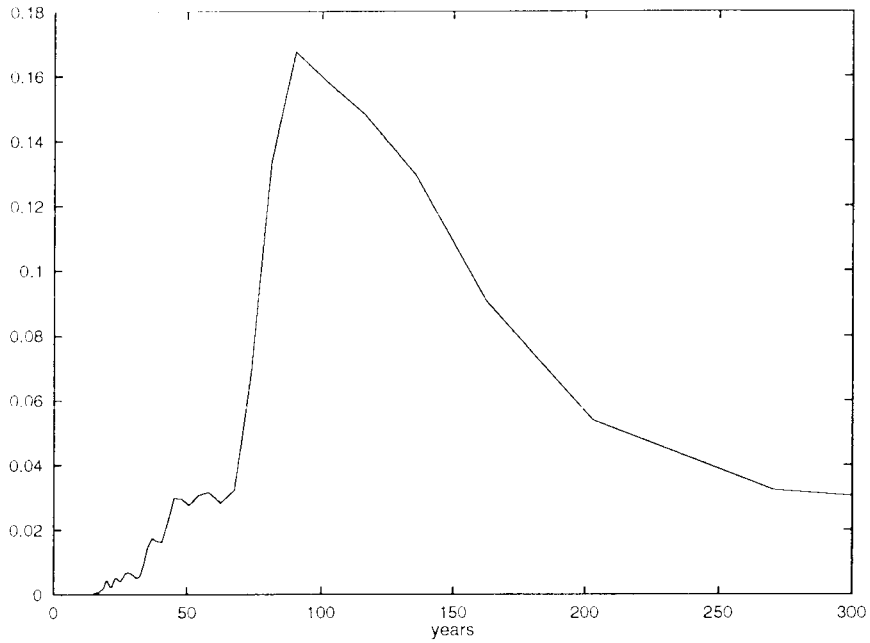

Figure 3.5: Power spectrum of the meridional heat transport. The multiplying limits for the 95 % confidence interval are 0.598 and 2.00.

in the spectra of other quantities, such as the surface averaged heat flux, meridional salt transport and the maximum of the overturning function.

In order to investigate the sensitivity of the response to the intensity of the stochastic forcing we repeated the above described experiment for several values of the standard deviation. The results are shown in figure 3.6. If the standard deviation is decreased by 50 % the variability in the meridional heat transport decreases with 50 %. Whereas an increase by a factor 2.5 results in a 10 % increase of the variability in the meridional heat transport. These results show, that there is a strong nonlinear dependence of the variability of the meridional heat transport on the strength of the stochastic forcing. As expected the sign of this dependence is positive. if the standard deviation becomes less 0.05 times the maximum of the original freshwater flux the

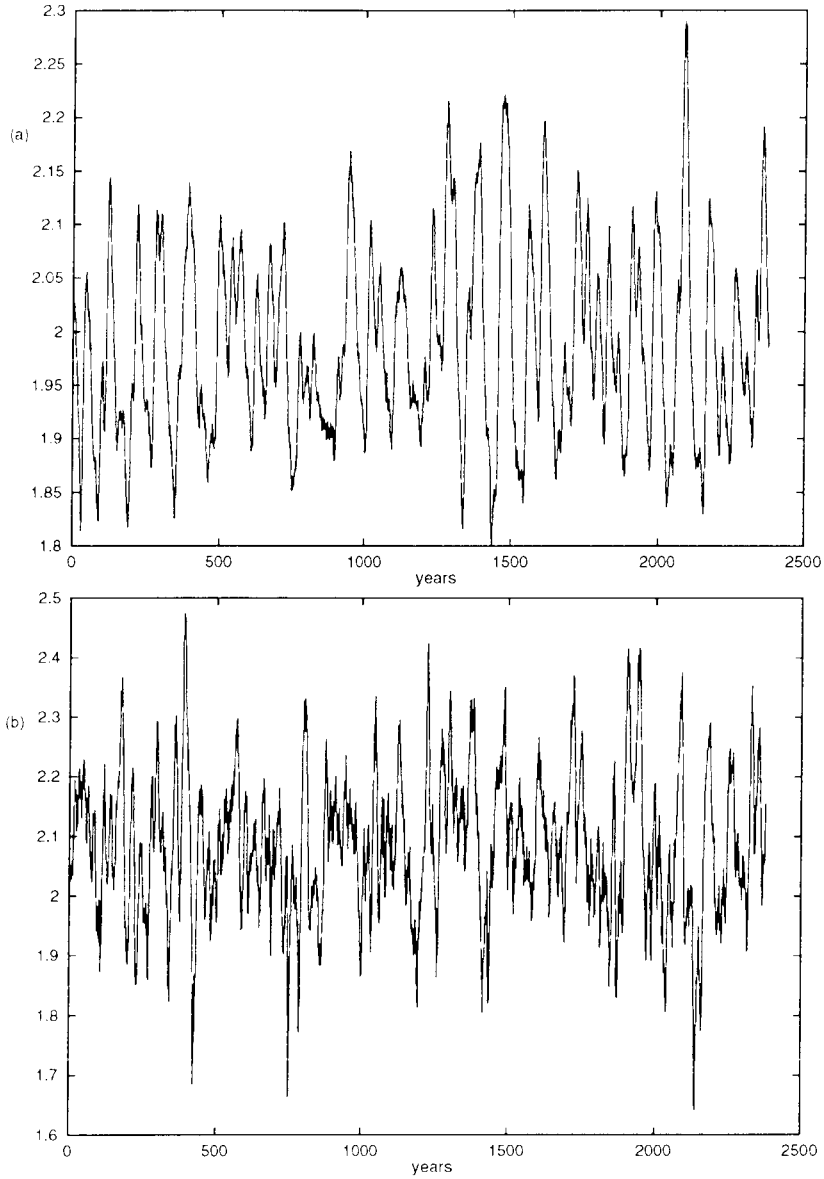

Figure 3.6: Time series of the meridional heat transport in 10^{14} at y=M/2 under a stochastic forcing of 20% (figure a) and 100% (figure b).

response of the system is only marginal. No real variability is perceptible with these intensities.

3.7 Comparison with theory

In order to investigate the value of the stochastic theory of Hasselmann (see section 2.1), the predicted spectrum is compared with the experimental found spectrum. The stochastic forcing component is implemented by a salt flux and therefore the meridional salt transport is the most appropriate quantity to use for comparison. In the experiment a stochastic component with a standard deviation of 0.4 times the maximum of the original freshwater flux is used. In equation 2.14 the constants λ_i have dimension time^{-1}. The value of these constants is unknown, but is related to the characteristic time scale of the variable y_i. In the experiments we found an oscillating behaviour of the ocean with a characteristic period in the order of a century and a logical choice for the λ of the meridional salt transport would thus be 1/100 years^{-1}. The constant F(0) is determined by matching the predicted spectrum with the experimental found spectrum. The result is shown in figure 3.7.

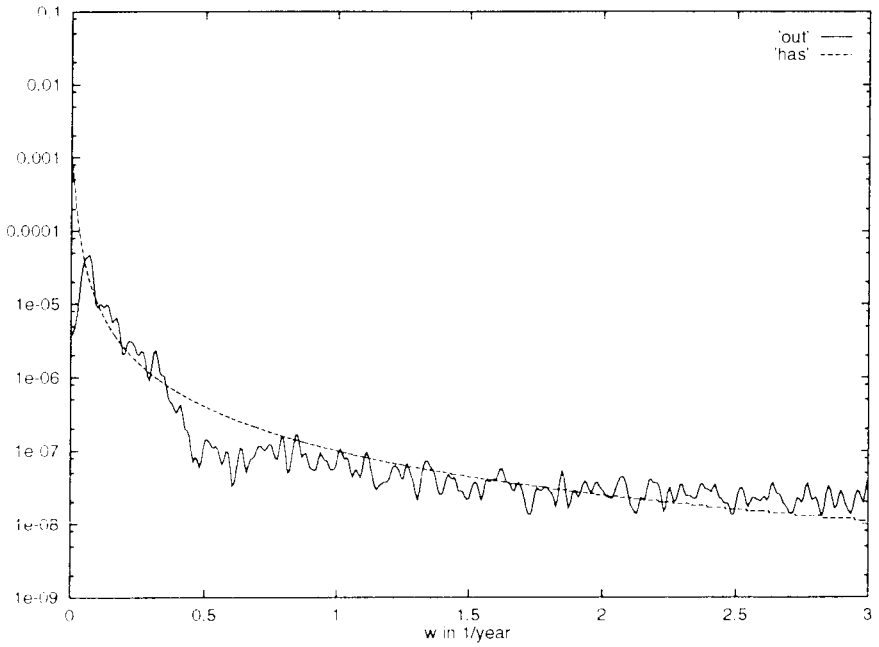

Figure 3.7: The meridional heat transport at y = M/2 in 10^{14} W under a stochastic forcing of 40 %.

The experimental found spectrum shows a peak around periods in the

order of a century, whereas the predicted spectrum reveals no peak at all. The theoretical approach is thus unable to explain the oscillating behaviour of the ocean. In the theoretical approach the assumption was made, that the system's evolution could be described by small fluctuations around a stable equilibrium and so implicitly assuming, that the ocean-atmosphere feedback could be modeled by linear relaxation of ocean quantities to prescribed values. In our model a stochastic component is added to the freshwater flux and if the relative importance of this term becomes large this assumption is no longer valid. In this experiment the relative importance of the stochastic component is quite large. It is also possible that the system's behaviour cannot be characterized by small fluctuations around an stable equilibrium, which is our basic assumption.

Chapter 4

Phase space description

Due to the complexity of the model it is not possible to solve the model equations analytically. Therefore a phase space description is used to deduce some important characteristics of our ocean-model and so making a qualitatively description of the evolution of the system possible. In a phase space description there are several representations, which can be used to describe the previous found oscillating behaviour. In this chapter the most likely phase space description will be determined with the aid of computer experiments.

4.1 Possible phase space descriptions

The spin-up state is used as starting point of the experiments. To test the stability of the spin-up state of the model an instantaneous perturbation is added to the freshwater flux. Thereafter the model is integrated for another 500 years. The spatial structure of this perturbation is given by $\sum_{\bar{\kappa}} Scos(\bar{\kappa} \cdot \bar{x} - \theta)$, with $\bar{\kappa} = (4\pi/\mathrm{L}, 0)$ and $(0, 4\pi/\mathrm{M})$. The constant S is determined by the restriction, that the maximum value of the perturbation is equal to 0.1 PSU (86mm evaporation per year). This experiment is repeated for the values $0, \pi/2, \pi$ and $3\pi/2$ of θ. In all of the experiments the spin-up appeared to be a stable equilibrium.

Using this result we consider 3 possibilities for the dynamics of the phase point.

1. *Fluctuations around stable equilibrium*
   The dynamical behaviour of the system is determined by one stable

equilibrium. The evolution of the system can be described by noise induced fluctuations around this equilibrium. The stochastic component of the freshwater flux is only necessary to get the system out of the equilibrium state and the evolution is mainly determined by the phase paths of the ocean-model. If the stochastic perturbation is switched off, the system will return to its original state.

It is also possible, that there is a group of stable equilibria, which are very similar and thus located close to each other in phase space. The existence of multiple equilibria in a similar ocean-model has already been established by Lenderink and Haarsma [10]. The dynamical behaviour of the ocean-model can then be described as fluctuations around these equilibria. This situation is not essentially different from the case, where there is only one stable equilibrium. After switching off the stochastic perturbation the system will return to one of the equilibria, which is of course not necessarily the spin-up state.

2. *Fluctuations between two or more stable equilibria*
   The dynamical behaviour of the system is determined by two or more stable equilibria, which are quite different and thus located at considerable distance in the phase space. The system's evolution can then be described by fluctuations around the equilibria and transitions between the equilibria. Due to the stochastic perturbations the system will make transitions between the different equilibria. After the stochastic perturbation has been switched off the system will go to one of the equilibria. The basic difference with the previous case is, that the different equilibria have quite different structures. It is again possible, that there are groups of equilibria, which are very similar, but this does not affect the characteristic picture of the dynamical behaviour of the system.

3. *Fluctuations between a stable and an unstable equilibrium*
   The dynamical behaviour of the system is determined by a stable and an unstable equilibrium. The evolution of the system can be described by fluctuations around the stable equilibrium and a transition to the unstable equilibrium. The latter is possible because an unstable equilibrium will in general only have a repelling force in a few directions in the phase space. The perturbation of the freshwater flux is necessary to get the system out of the attraction area of the stable equilibrium into that of the unstable one. The return to the stable equilibrium is

fairly easy to trigger. After the stochastic perturbation is switched off the system will move either towards the stable or unstable equilibrium. If the system is close to the unstable equilibrium a small perturbation will be sufficient to realize a transition to the stable equilibrium.

There may be several unstable equilibria, but this will not change the main characteristics of the dynamical behaviour. Also it is possible, that there are various stable equilibria. The dynamical behaviour of the system is then characterized by transitions between stable equilibria and between stable and unstable equilibria. The basic view becomes more complicated, but is not essentially different from the case with only one stable and one unstable equilibrium. Again it is possible, that there are groups of similar equilibria.

4.2 Sensitivity of the model's behaviour to the external forcing

In order to obtain a better understanding of the internal dynamics of the system one oscillation is examined in more detail. The starting point of the experiment is again the spin-up state and during the integration a stochastic component is added to the freshwater flux with a standard deviation of 40 percent of the original maximum of the freshwater flux (see section 3.5). In order to get a substantial oscillation soon after the beginning of the experiment, the series of random phases ϕ is shifted. All other parameters and boundary conditions are the same as in the spin-up experiment. The experiment lasted for 5500 model steps, which is equivalent with about 87.2 years.

To compare the importance of the noise to the importance of the internal dynamics of the system, the above described experiment is repeated several times. In each of these integrations the stochastic component of the freshwater flux is switched off at a different time. The results are shown in figure 4.1.

By looking at the figure one can conclude, that substantial variability in the system's behaviour is possible and therefore it seems, that the influence of the stochastic perturbation on the behaviour of the system is quite critical.

If the stochastic perturbation is switched off in the interval (15.9-17.8 years), we see a substantial decrease of the meridional heat transport in comparison to the integration with the stochastic perturbation on. Without the stochastic perturbation the system's behaviour does not display the original oscillation. Instead the system seems to converge to an equilibrium with a much weaker meridional heat transport than the spin-up state.

On the other hand when the stochastic perturbation is switched off a few years later in the interval (24.6-27.7 years) the system's behaviour closely resembles that of the original integration. And so once the oscillation has started the influence of the stochastic perturbation appears to be limited.

The influence of the stochastic perturbation in the interval (18.2-21.4 years) seems to be weaker than in the interval (15.9-17.8 years), but stronger than in the previous interval. The oscillation is also not captured without the stochastic forcing, but the meridional heat transport no longer shows a large decrease. After turning off the external forcing the system seems to converge slowly to the original spin-up state. The role of the stochastic perturbation in this interval is thus still important, but in contrast to the

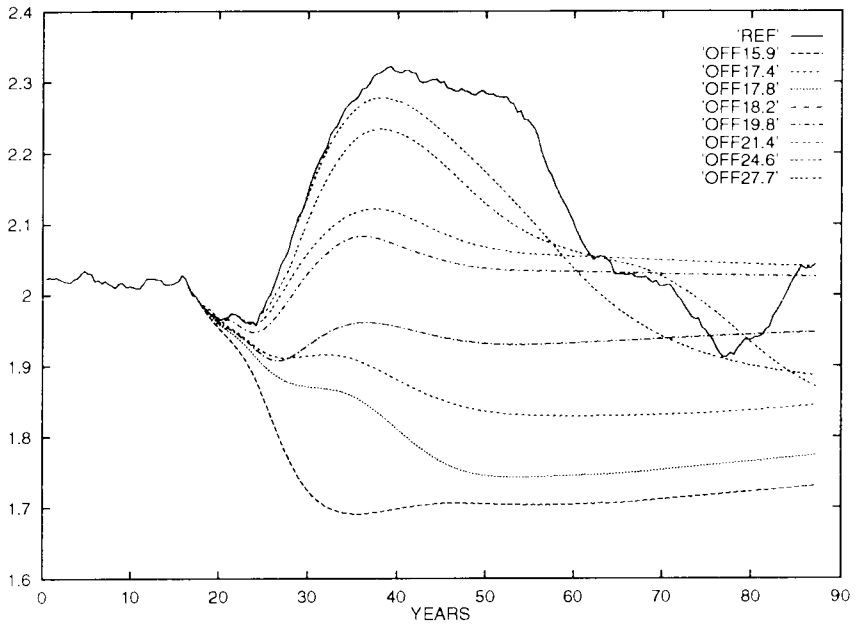

Figure 4.1: The meridional heat transport at y = M/2 in 10^{14} W for the integrations, where the stochastic perturbation is left on (solid line) and switched off at several times (dashed lines).

interval (15.9-17.8), where the system appears to be in a very sensitive state, the influence of the external forcing is to push the system slowly in a specific direction.

This variety in the behaviour of the ocean-model is not only present in the meridional heat transport, also other quantities show the same kind of behaviour (see figure 4.2).

From these experiments we are able to conclude, that the first of the three possible phase space descriptions as described in the previous section is rather unlikely. In this case one would expect, that the stochastic perturbation would only cause minor deviations of the original phase paths. In this experiment however we found a substantial variety in the behaviour of the system, when the external forcing was switched off at different times. In addition the system seems to converge to a new equilibrium depending on the time, when the stochastic forcing is switched off. It is however possible, that the stochastic perturbation is strong enough to get the system far from the equilibrium, thereby decreasing the attraction of that equilibrium. In this situation the relative importance of the stochastic perturbation is increased and so the stochastic perturbation could indeed play an important role in the dynamical behaviour of the model.

The second possibility with two stable equilibria, which are located at considerable distance in phase space, seems more likely. In this case the dynamical behaviour of the system could be characterized by fluctuations around and transitions between these equilibria. To realize a transition between two equilibria the stochastic perturbation plays a critical role. It forces the system out of the attraction area of the first equilibrium into that of the second. If the system is close to the separatrix of the attraction basins, the external forcing plays a decisive role in the behaviour of the system. This could explain the variety in the possible behaviour of the model in the interval (15.9-17.8). If the system is close to an equilibrium the influence of the external forcing is limited and the dynamical behaviour of the system is determined by the phase paths, which would explain the behaviour of the model in the interval (24.6-27.7).

The third possibility with a stable and an unstable equilibrium is also possible. The behaviour of the ocean-model would then be determined by fluctuations around the stable equilibrium and between the stable and unstable one. The influence of the stochastic perturbation in this situation is critical. Not only is it necessary to cause a transition between the stable and unstable equilibrium, when the system is close to the unstable equilibrium the system is very sensitive to a stochastic perturbation. The behaviour of

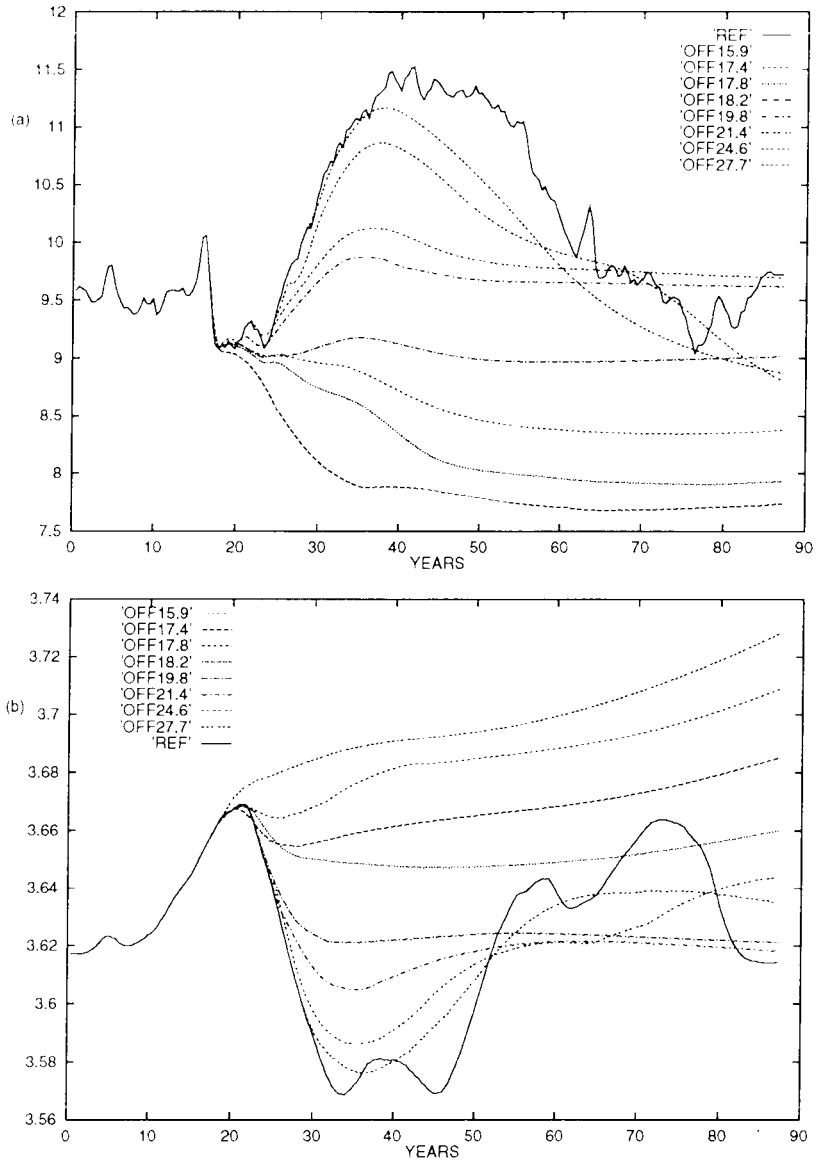

Figure 4.2: The behaviour of the system, when the stochastic perturbation is left on during the whole integration (solid line) and switched off at different times (dashed lines). a: Maximum of the overturning function in Sverdrups, b: Temperature in °C of the deepest layer of the ocean, averaged over the top 1250 km of the basin.

the model in the interval (15.9-17.8) is in accordance with this idea.

4.3 Different equilibria

In order to obtain a better understanding of the dynamics of the system, we integrated the model for much longer time. With this experiment we wanted to answer the following questions:

Does the model gradually converge to the same equilibrium in all of the cases ? In this case the phase space will probably contain only one stable equilibrium.

Or does the model converge to different equilibria for different switch-off times ? If so, the previously discussed possibilities 2 and 3 are more likely.

From each of the three intervals one example is taken and the model is integrated for another 1500 years. The results are shown in figure 4.3. In the

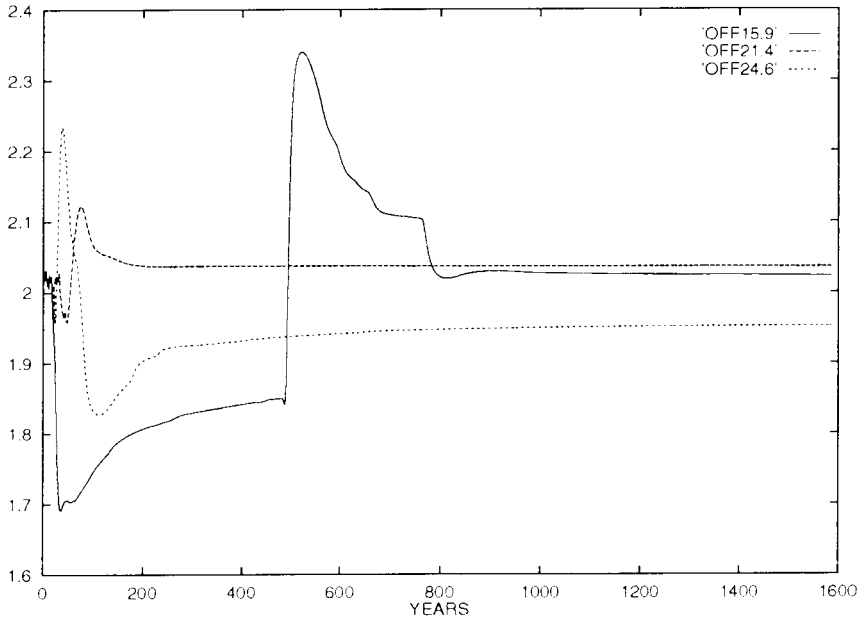

Figure 4.3: Time series of the meridional heat transport at y = M/2 in 10^{14} W under a stochastic perturbation with a standard deviation of 40 %, when the stochastic perturbation is switched after 15.9, 21.4 or 24.6 years.

cases, when the stochastic perturbation is switched off after 15.9 respectively

21.4 years, the model seems to converge to the original equilibrium. Not only the meridional heat transport converges to the value of the original equilibrium, also several other quantities, such as the meridional overturning and the meridional salt transport approach their value of the spin-up state. If however the stochastic perturbation is switched off after 24.6 years the model does not converge to the spin-up state. This suggests, that there are at least two equilibria, which are important for the dynamical behaviour of the system.

If we look at the time series of the case, when the stochastic perturbation is switched off after 15.9 years, we see a sudden jump in the meridional heat transport after about 500 years of integration. This phenomenon can be explained by assuming that there is an unstable equilibrium. The stochastic perturbation of the freshwater flux during the first 15.9 years of the integration forced the system out of the attraction basin of the original equilibrium into that of the unstable one. If the system comes closer to the unstable equilibrium, the repelling force of the unstable equilibrium becomes stronger. When the repelling force becomes too strong, the system rapidly moves away from the unstable equilibrium and returns to the spin-up state.

In the experiment the transition is rather sudden. From theory one would expect a more smoother curve. This is probably due to the way convection is parameterized in our ocean-model. Convection occurs, when the stratification of two adjacent layers is unstable. The two layers, or parts of them, are then mixed to get a stable stratification. In this model convection is parameterized by a step-function. Complete mixing occurs, when the layers are unstablely stratified. No mixing takes place in stable condition. Therefore, a possible explanation for the sharp edge in the time series of the last experiment would be, that prior to this point the stratification slowly becomes less stable and finally becomes even weakly unstable. In our model this implies, that prior to this point no convection occurs and then suddenly convection is switched on resulting in a sharp edge.

If the stochastic perturbation is switched off after 24.6 years, the model seems to converge to a different equilibrium. To investigate the stability of this equilibrium the model is integrated for another 1000 years. At the begin of the integration an instantaneous perturbation is added to the freshwater flux. The structure of this perturbation is described in section 4.1. The constant S is again chosen such that the maximum value of the perturbation is equal to 0.1 PSU (86 mm evaporation per year) and θ is chosen to be $-\pi/2$. The result is shown in figure 4.4. After the perturbation has been applied, the system undergoes an oscillation and finally returns to the spin-

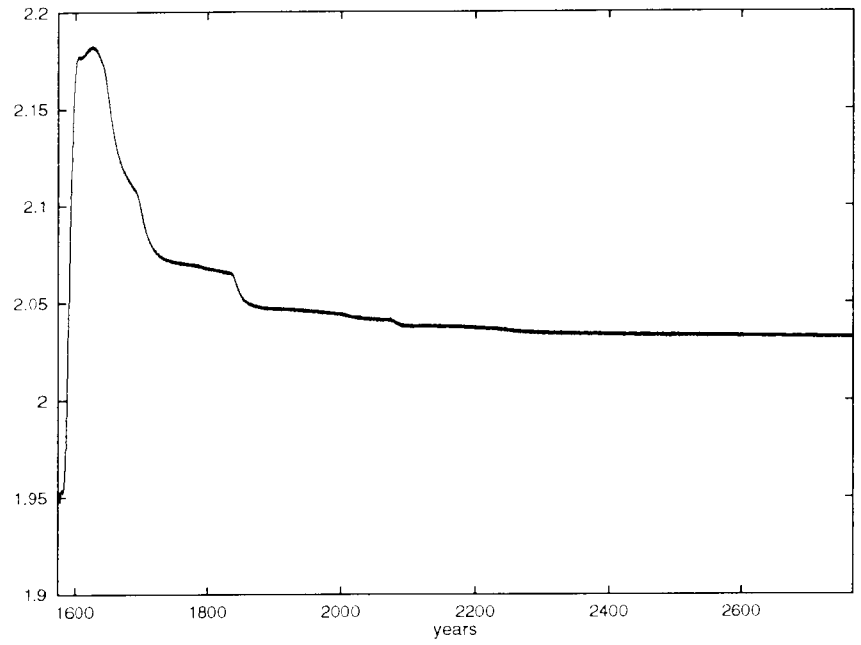

Figure 4.4: Time series of the meridional heat transport at y = M/2 in 10^{14} W, when an instantaneous perturbation is added to the freshwater flux at the beginning of the integration.

up state. A small perturbation is sufficient to cause a substantial jump in the meridional heat transport. Apparently the system is in a sensitive state, yielding the conclusion, that the system does not converge to a stable equilibrium. This result also supports a phase space description with one stable and at least one unstable equilibrium.

4.4 Spectra analysis

In the case of a stable equilibrium together with at least one unstable equilibrium one would expect an increase in the possibility of escaping the attraction basin of the stable equilibrium if the intensity of the stochastic perturbation is increased. When the intensity of the stochastic perturbation is increased the time between two consecutive transitions between a stable and an unstable equilibrium should therefore decrease and hence the characteristic period (see section 3.6) should also decrease. In this experiment we integrate the model three times for a period of 8000 years. In each of the integrations an additional stochastic perturbation is added to the freshwater flux. The standard deviation of the stochastic perturbation is 20 %, 40 % respectively 100 % of the original maximum of the freshwater flux. From each of these three integrations a power spectrum of the meridional heat transport is made. The results are shown in figure 4.5.

The confidence intervals of the spectra are quite large. The differences between the spectra are therefore not significant. Nevertheless we will still use the spectra for comparison. If we look at the characteristic period in each of the cases, we see that the characteristic period does not change in the predicted way. By increasing the standard deviation from 20 % to 40 % the characteristic period indeed decreases, which is in accordance with our expectations. A further increase of the standard deviation however results in an increase of the characteristic period. This result is in contradiction with the theory and is also not in accordance with any of the other possible phase space descriptions. A possible explanation for this phenomenon could be, that if the standard deviation of the stochastic perturbation is increased from 40 % to 100 % additional equilibria become important for the dynamical behaviour of the model. These equilibria should be located at considerable distance from the spin-up state in the phase space. The transition time to these equilibria from the spin-up state is large, resulting in an increase of the characteristic period.

Another possibility is, that the spectra are indeed not reliable enough to

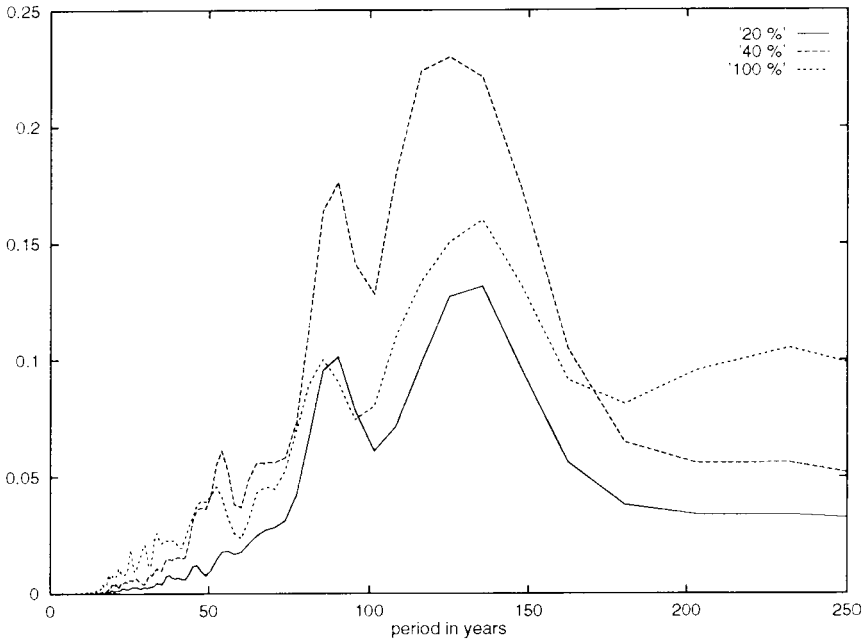

Figure 4.5: Power spectrum of the meridional heat transport for a standard deviation of the stochastic perturbation of 20 %, 40 % and 100 % of the maximum of the original freshwater flux. The multiplying limits for the 95 % confidence interval are 0.634 and 1.807.

use for comparison. To check this possibility the model was integrated for 20000 years under a stochastic perturbation of the freshwater flux with a standard deviation of 40 %. The time series of the meridional heat transport of this experiment was split in two parts. From each of these parts a power spectrum was made and the result is shown in figure 4.6.

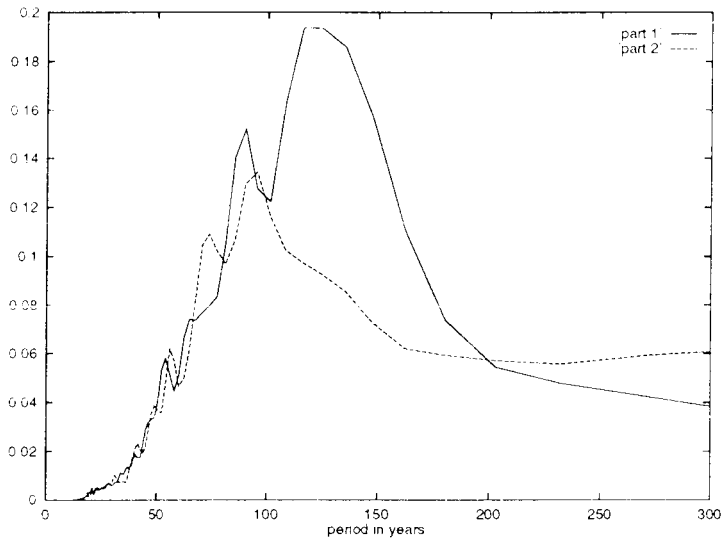

Figure 4.6: Comparison of the power spectra of the meridional heat transport for a time series, which is split in two. The multiplying limits for the 95 % confidence interval are 0.674 and 1.637.

By comparing the spectra of both parts, we see a substantial difference. Although the differences are not significant an estimation of the characteristic period would give in each of the cases a different period. Apparently the method of comparing characteristic periods for different values of the standard deviation of the stochastic perturbation is not reliable enough to conclude which phase space description is the most likely.

4.5 Approximating an unstable equilibrium

The phase space description with a stable equilibrium and at least one unstable equilibrium seems the most appropriate theory to describe the system's behaviour. In order to get more support for this theory a minimization procedure is used to try to find an unstable equilibrium numerically. The ocean-circulation is driven by density gradients and the windstress. The windstress is known and constant in time. Therefore the following functional F is defined

$$F = C \cdot \int\int\int_V \frac{\partial \rho}{\partial t} \cdot \frac{\partial \rho}{\partial t} dV, \tag{4.1}$$

where C is a scaling constant. The zero points of this functional correspond to the points, where $\frac{\partial \rho}{\partial t} = 0$. Through the hydrostatic approximation (see section 3.2) it immediately follows, that a constant density field implies a constant pressure field. The velocity field is also stationary if the pressure field is constant in time. From the equation of state it follows, that

$$\frac{\partial \rho}{\partial t} = \alpha_S \frac{\partial S}{\partial t} + 2\alpha_T (T - T^*) \frac{\partial T}{\partial t}. \tag{4.2}$$

Thus, a constant density field does not imply a constant salinity and temperature distribution. Nevertheless, we will try to minimalize the functional F and check afterwards whether the salinity and temperature distributions are also stationary.

In our model convection is parameterized by a step-function, i.e. no convection occurs until the vertical stratification becomes unstable. This implementation introduces a discontinuity in equations 3.8 and 3.9. This discontinuity complicates the minimization of the functional F. Therefore for this minimization procedure the step-function is replaced by a continuous function. This function is defined as:

$$f(\rho, k) = \begin{cases} 0 & \text{if } \rho(k) - \rho(k+1) \leq -g(k) \\ 1/2 + 1/2 * sin(\frac{\pi}{2g(k)}(\rho(k) - \rho(k+1))) & \\ & \text{if } |\rho(k) - \rho(k+1)| < |g(k)| \\ 1 & \text{if } \rho(k) - \rho(k+1) \geq g(k) \end{cases} \tag{4.3}$$

The value of the function $f(\rho, k)$ determines the part of the layers k and $k+1$, which is mixed. Still no mixing occurs if the stratification is absolutely stable and complete mixing if the stratification is very unstable, but a transition interval is introduced for intermediate stratifications. If

the stratification is only marginally stable (or unstable) a part of the layers k and $k+1$ is mixed. The function $g(k)$ is a height dependent function, which is constant in each layer and determines the length of the transition interval. Its value decreases with increasing k to account for the fact, that the density differences between the lower layers are less than those between the upper layers. The function g(k) is found by matching the behaviour of the system under a stochastic perturbation using the old convection scheme to that using the new scheme. The function $f(\rho, k)$ is a continuous function and also its derivative is continuous. Its second derivative is however is discontinuous. This is still a complication for the minimization process, which could be solved by replacing $f(\rho, k)$ by an arctangent. An arctangent however would introduce some additional diffusion in the system, i.e. there would still be some mixing even if the system is absolutely stable. Therefore the arctangent function is not used.

The functional F cannot be computed analytically, because the 3-dimensional field $\frac{\partial \rho}{\partial t}$ is not exactly known. The values of this field are known in each grid point and so F is approximated by

$$\hat{F} = \sum_{i=1}^{N} C \cdot (\frac{\partial \rho_i}{\partial t})^2, \tag{4.4}$$

with N the number of grid points.

As minimization procedure the NAG library E04DGF is used. This routine uses a pre-conditioned conjugate gradient method. It is intended for large scale problems and uses limited memory. The search direction is obtained by a quasi-Newton method. This is an iterative method, which means that an initial guess for the zero point of F is needed. The initial guess is an important factor for the success of the method. The better this initial guess is, the better this method will work. We thus need an initial guess, which is in the vicinity of the unstable equilibrium we want to find.

In order to obtain a proper initial guess, we again consider the experiments performed in section 4.2 and 4.3. In these sections an experiment was performed where we switched off the stochastic perturbation at several times. In the integration, when the stochastic forcing is switched off after 15.9 years, there was a sudden jump in the meridional heat transport (figure 4.3) after about 500 years of integration. This behaviour could be explained by assuming, that the system was close to an unstable equilibrium at that point. Our goal is to find an unstable equilibrium, so this point could serve as an initial guess.

We adjusted however the convection scheme and this could influence the equilibria of the system. Therefore to be completely fair this experiment was repeated with the new convection scheme, while all the other parameters and boundary conditions were left unchanged. The result is shown in figure 4.7. The difference in the system's behaviour is small during the first 500 years of integration. After 500 years there is a substantial difference in the system's

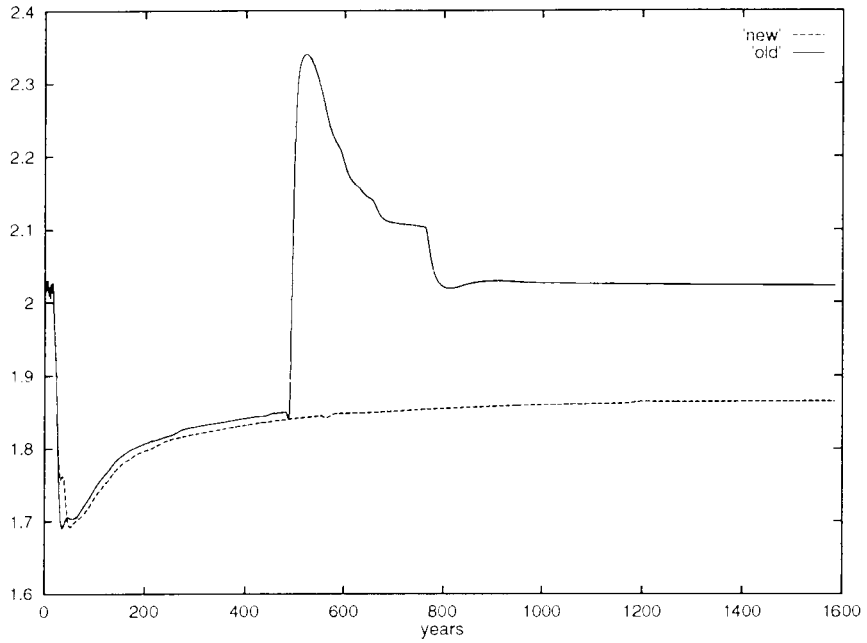

Figure 4.7: The meridional heat transport at y=M/2 in 10^{14} W, when the stochastic perturbation is switched off after 15.9 years using the old (solid line) and new convection scheme (dashed line). The standard deviation of the stochastic perturbation is 40 % of the maximum of the original freshwater flux.

behaviour. The jump in the meridional heat transport does not occur when the new convection scheme is used. The new convection scheme introduces a small amount of mixing in situations, where the system is only marginally stable. This makes the system slightly more stable and prevents the jump. If however a small instantaneous perturbation is added to the freshwater flux at the end of the integration the jump almost immediately takes place. The state of the system at the end of the integration with the new convection scheme seems therefore to be a good initial guess. The temperature and

salinity distributions of this point will be used as an initial guess in our minimization process.

The NAG library requires the first derivatives of the functional F. This derivative cannot be computed exactly and therefore it is computed in each grid point numerically using a central differencing scheme. The step-size for this differencing scheme is chosen to be constant in each grid point. Computing the derivative of F numerically makes however the minimization process very costly. Therefore the minimization process is stopped after 60 iterations. The result is shown in table 4.1.

	functional F	salinity comp.	temperature comp.
begin	2.7628	0.90967	$7.065 \cdot 10^{-3}$
end	$2.8469 \cdot 10^{-3}$	5.9797	$8.6844 \cdot 10^{-3}$

Table 4.1: Values of the functional F (column 1), the salinity component of the functional (column 2) and the temperature component of the functional (column 3) before and after the minimization procedure.

The minimization routine seems to converge to an equilibrium as the functional F is decreased by a factor of about thousand (column 1). In order to check if the salinity and temperature distribution are also stationary the terms

$$C \cdot \int\int\int_V \alpha_S^2 \frac{\partial S}{\partial t} \cdot \frac{\partial S}{\partial t} dV \quad \text{and} \quad C \cdot \int\int\int_V \alpha_T^2 \frac{\partial T}{\partial t} \cdot \frac{\partial T}{\partial t} dV$$

are computed numerically.

These terms are also given in table 4.1 (column 2 and 3). There is a substantial increase of both terms by the minimization process, yielding the conclusion, that apparently the salinity and temperature distributions have not become stationary. Thus, the point, which is obtained by minimizing the functional, is not an equilibrium point of the whole system. The final point is a point with a stationary density distribution. The temperature and salinity distributions are not stationary, but vary in such a way that the distribution remains constant.

By minimizing the functional F we were not able to find an equilibrium point of the system. The salinity and temperature distributions did not become stationary. Therefore a new functional G,

$$G = \int\int\int_V (C_1 \cdot (\frac{\partial S}{\partial t} \cdot \frac{\partial S}{\partial t}) + C_2 \cdot (\frac{\partial T}{\partial t} \cdot \frac{\partial T}{\partial t})) dV, \tag{4.5}$$

is defined. The constant C_1 and C_2 are scaling constants and make sure, that both components of the functional are equally important. The zeros of this functional correspond to the points with a stationary salinity and temperature distribution. These points are thus equilibrium points of the system. Again the functional cannot be computed analytically and is therefore approximated by

$$\dot{G} = \sum_{i=1}^{N} C_1 (\frac{\partial S_i}{\partial t})^2 + C_2 (\frac{\partial T_i}{\partial t})^2, \tag{4.6}$$

with N the number of grid points. The same method is used to minimize the functional G as for the functional F. The derivative of G is also computed numerically using central differencing. The initial guess remains the same and the maximum number of iterations is set to be 65. The results are shown in table 4.2.

	funct. G	sal. comp.	temp. comp.	low sal.	low temp.	Deriv.
begin	3.111	1.519	1.592	0.2564	0.09360	41.25
end	0.2632	0.06394	0.1993	$0.476 \cdot 10^{-2}$	0.01249	15.366

Table 4.2: Values of the functional G (column 1), salinity component of the functional (column 2), the temperature component of functional(column 3), the salinity component of the functional for the southern half of the basin (column 4), the temperature component of the functional for the southern half of the basin (column 5) and the Euclidean norm of the derivative of G (column 6) before and after the minimization procedure.

The minimization process is terminated after only 46 iterations due to lack of convergence, i.e. the functional G (column 1) is only reduced by a factor of about 10. The main cause of this lack of convergence is the disability of the minimization routine to substantially decrease the Euclidean norm of the derivative of G (column 6). By minimizing the functional G the salinity and temperature component of G (column 2 and 3) are indeed decreased, but only by a factor of about 10.

This minimization procedure was repeated with a different initial guess. To obtain this initial guess we again considered the experiments performed in sections 4.2 and 4.3. When the stochastic perturbation was switched off after 24.6 years the system slowly seemed to converge to an equilibrium different from the spin-up state (see figure 4.3). If however after 1600 years

of integration an instantaneous perturbation is added to the freshwater flux, a substantial jump in the meridional heat transport almost immediately takes place. The state of the ocean after 1600 years was therefore used as another initial guess for finding an unstable equilibrium. The results were however very similar.

The disability to substantially decrease the Euclidean norm of the derivative of the functional G may have several causes. The scaling constants C_1 and C_2 in the functional G are determined by the restriction, that the salinity component and the temperature component have the same size at the beginning of the minimization procedure. The choice of the scaling constants was however fairly arbitrary. A different choice of the scaling constants could therefore result in a better convergence of the minimization of the functional G. Further, the derivative of G is computed in each grid point numerically using a central differencing scheme. This is not only very costly, it may also not be very accurate. The accurateness of this method strongly depends on the step-size, which is used in the differencing scheme. In this experiment the step-size was kept constant and it may be necessary to adjust the step-size at different grid points. A third problem is the way convection is parameterized in the model. Convection was parameterized by a step-function, thereby introducing a discontinuity in the equations for salinity and temperature. In order to get rid of this discontinuity the step-function was replaced by a continuous function (see equation 4.3). A height dependent sine function was used to make the transition from no mixing (stable stratification) to complete mixing (unstable stratification) continuous. The length of this transition interval is determined by the function $g(k)$ and decreases with increasing k. The function was obtained by matching the behaviour of the model using the old convection scheme to that using the new convection scheme, thereby making the transition interval very small. The smaller this interval is, the more steep the derivative of the function $f(\rho, k)$ becomes. Numerically computing the derivative in this interval using a central differencing scheme is extremely sensitive to the step-size. This could be an explanation for the fact, that the Euclidean norm of the derivative remains large. The step-function was replaced by a continuous function with a continuous derivative, but the second derivative is discontinuous. This is also an additional problem for the minimization process.

The northeastern part of the basin is the area, where deep convection takes place. In this area there will be probably several regions, where the stratification is only marginally stable or unstable. Therefore one expects, that the large gradients of the functional G are located in this area. In

order to check this hypothesis the salinity and temperature component of the functional G are computed for the southern half of the basin. The results are also shown in table 4.2 (column 4+5). This salinity term is decreased by a factor of about 50 and the temperature term by a factor 8. The minimization process has thus also not been able to substantially decrease these terms. The relative importance of these terms to the salinity and temperature component of G for the whole basin is however small. This supports the theory that the greatest problems for the minimization process are located in the convective area.

In order to further investigate this theory it would be interesting to numerically search for an equilibrium point of the model when convection is neglected. If the minimization process is unable to find an equilibrium point of the system, the problems are not totally located in the convective area. Finding an equilibrium point of the system by the minimization routine will on the other hand supports this theory. If the minimization routine is able to find an equilibrium point of the system, when convection is neglected, a different approach should be used for the original problem. One could adjust the convection scheme by enlarging the transition interval, thereby decreasing the large gradients of the functional G. This could however critically influence the behaviour of the model. If, due to convergence restrictions, the influence of the adjustment on the behaviour becomes too large, one could try a different minimization technique or functional. Probably a functional with a weight function, which decreases the relative importance of the convective area, would be a recommendable option to try. The problem of numerically finding an equilibrium point of the model is thus rather difficult. Due to lack of time we were not able to explore the above mentioned possible explanations for the failure of the minimization method.

4.6 Finding a proper distance function

The experiments performed so far indicate that the oscillating behaviour of the system under a stochastic perturbation of the freshwater flux is most likely described by a phase space description with one stable and at least one unstable equilibrium. For the description of the evolution of the system in the phase space therefore the distance of the state of the system to these equilibria could be used. In order to determine the distance of the actual state of the ocean to the equilibria, the exact location of these points should however be known. The spin-up state can be considered as a stable equilibrium. The exact location of the unstable equilibrium is however rather uncertain and can only be estimated. For the minimization process in the previous section we used two initial guesses and these points will be used as approximation for the unstable equilibrium, i.e. the state of the ocean just before the jump in the meridional heat transport, when the stochastic perturbation was switched off after 15.9 years and the state of the ocean after 1600 years, when the stochastic perturbation was switched off after 24.6 years.

In order to measure the distance of the state of the ocean to each of these equilibrium points it is necessary to define a proper distance function. The choice for this distance function is not a priori obvious. If the unstable equilibria are indeed important for the dynamical behaviour of the system, the system's behaviour can be characterized by fluctuations around the stable and transitions to the unstable equilibria. In case of a proper distance function the distance of the state of the system to the spin-up state should be smaller than the distance to the other equilibria if the system fluctuates around the stable equilibrium . When the system however is close to the unstable equilibrium the distance of the actual state of the system to the unstable equilibria should be the smallest.

Several distance functions were tried and analyzed afterwards. The experiment described in section 4.2 is repeated and time series of the distances to each of the equilibria are made. The time series of the meridional heat transport is displayed in figure 4.8.

So one oscillation is studied in detail. First the distance function, which is related to the meridional overturning is used, i.e.

$$d_{over} = \sqrt{\sum_{i=1}^{P} (\Phi_i - \Phi_{ieq})^2} \tag{4.7}$$

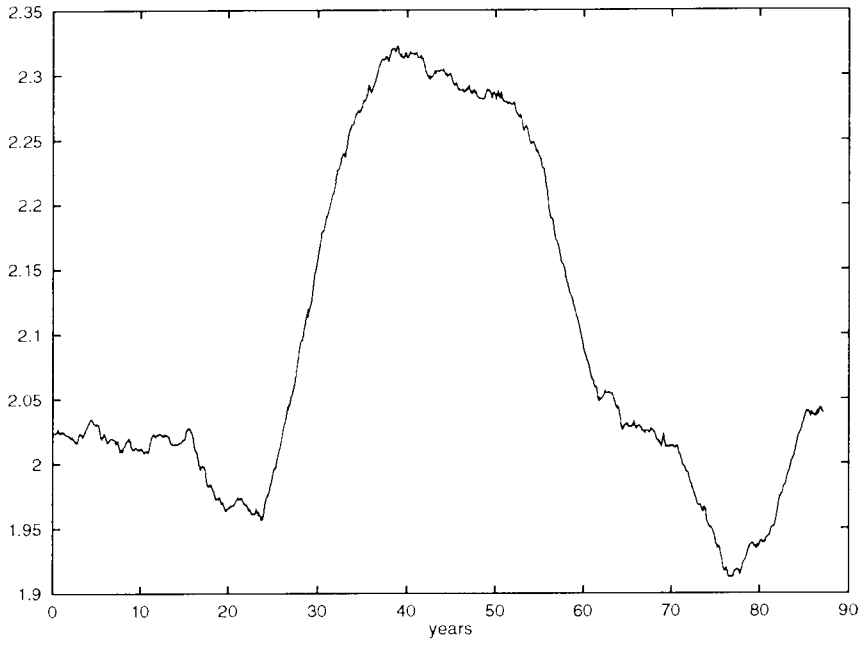

Figure 4.8: Time series of the meridional heat transport in 10^{14} at y=M/2 W under a stochastic perturbation of the freshwater flux with a standard deviation of 0.4 times the original maximum of the freshwater flux.

where P is the number of grid points used in the meridional direction times the number of grid points used for the depth of the ocean, Φ_i and $\Phi_{i,q}$ are the values of the meridional overturning function in a grid point of the actual state of the ocean and in the equilibrium point. The result is shown in figure 4.9.

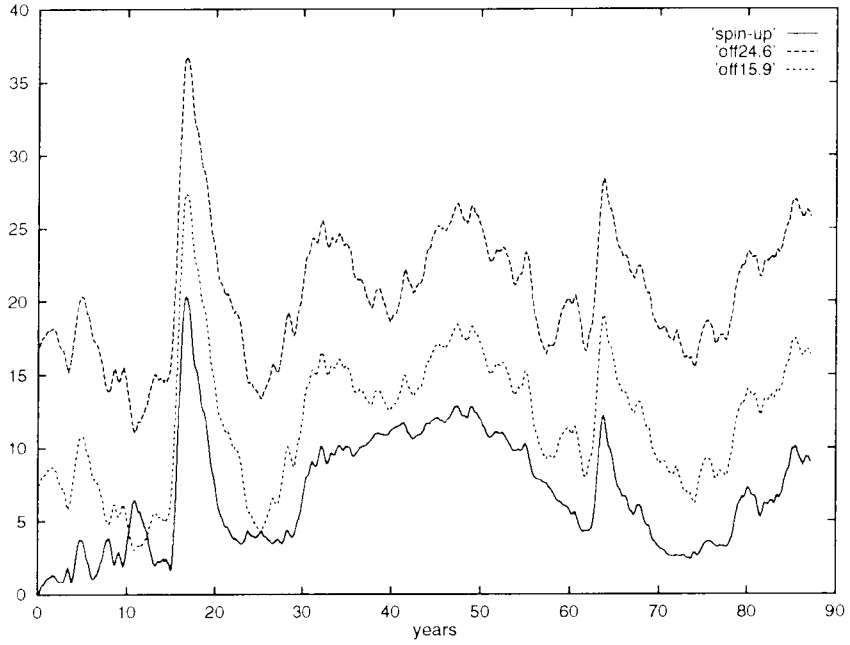

Figure 4.9: Time series of the distance to the equilibria using the distance function related to the meridional overturning function.

One expects, that the transition from the stable to the unstable equilibrium and back is responsible for the oscillating behaviour of the meridional heat transport. Because only one oscillation is considered, one expects that only during one period of time the state of the system will be closer to the unstable equilibria than to the spin-up state.

The time series of the distances to each of the equilibria show, that the actual state of the ocean is during almost the whole integration closer located to the spin-up state than to the other equilibria. Only after about 10 years the distance to the unstable equilibrium is during a brief period less than to the spin-up state. At that point the system is close to an unstable equilibrium and soon afterwards rapidly moves away from this equilibrium. When the system moves to the unstable equilibrium the distance of the

system's state to this point will indeed decrease. When it however comes to close to the equilibrium, the system will rapidly move away The obtained result is in accordance with this idea. The state of the system is however only during a very brief period of time closer located the unstable equilibria than to the spin-up state. One would expect however, that if the system is moving away from the unstable equilibrium, the distance of the system's state to the unstable equilibrium will during a somewhat longer period remain less than the distance to the spin-up state. It is possible that our view of the behaviour of the system in the phase space is not correct, it might however also be, that the chosen distance function is not capable of properly describing the evolution of the model in the phase space.

Therefore a second distance function, which uses the surface heat flux, is tried, i.e.

$$d_{hf} = \sqrt{\sum_{i=1}^{M} (hf_i - hf_{ieq})^2} \tag{4.8}$$

where hf_i and hf_{ieq} are the heat flux in a grid point of the actual state of the ocean and in the equilibrium point and M the number of surface grid points. The results are shown in figure 4.10a and b.

Using this distance function the actual state of the system is indeed during a longer period closer to the unstable equilibria (see figure 4.10). The state of the system is however during four periods of time closer to the unstable equilibria than to the spin-up state. This seems a little bit unrealistic and is also not in accordance with the above described theory. The value of this distance function seems therefore to be small

Variations in the surface heat flux are however strongly related to variations in the freshwater flux (see section 5.1.3). A stochastic perturbation is added to the freshwater flux and so there will be substantial variability in the surface heat flux on a short time scale. Therefore this will probably not be a very useful quantity for defining a distance function, which should describe the evolution of the total system. The meridional overturning function on the other hand slowly adapts itself to variations in the state of the ocean. This quantity seems more appropriate to define a distance function, but it may however adapt to slowly. A third distance function, which is related to the salinity distribution of the ocean is therefore tested, i.e.

$$d_S = \sqrt{\sum_{i=1, i \notin M}^{N} (S_i - S_{ieq})^2} \tag{4.9}$$

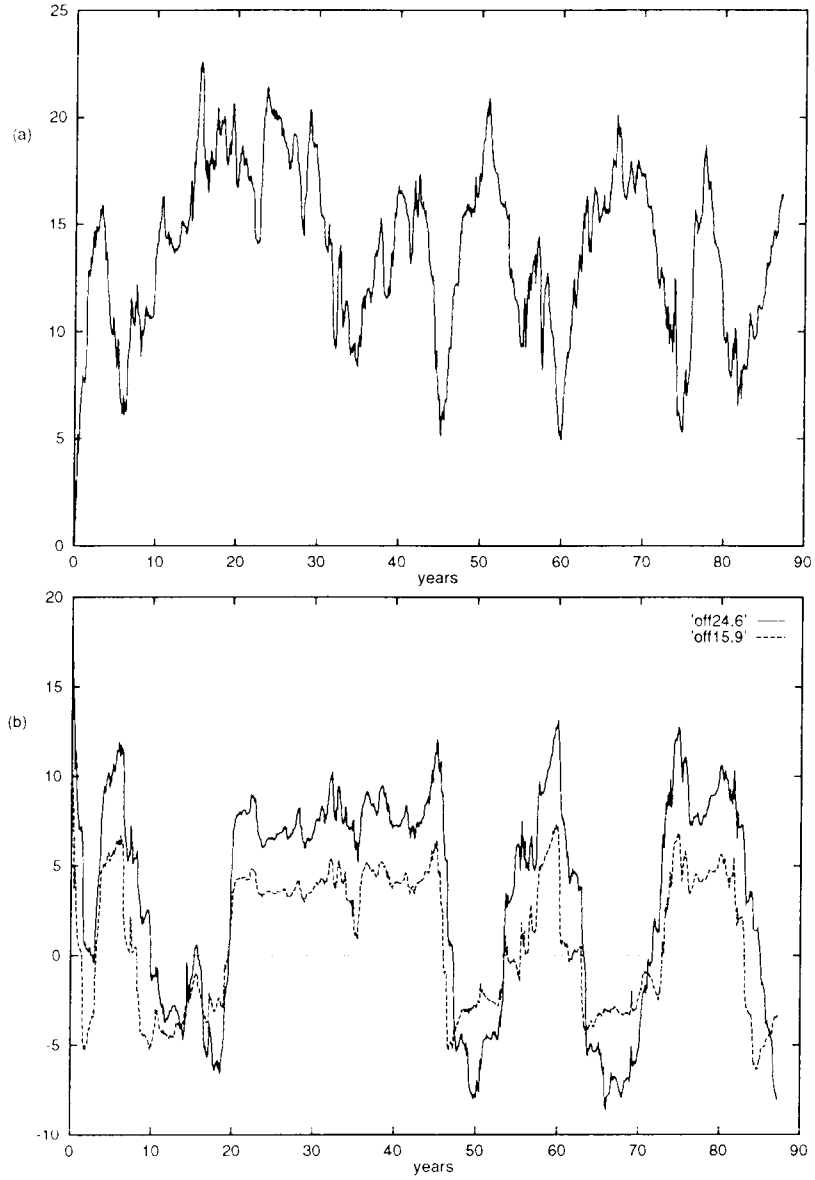

Figure 4.10: Time series of the distance to the equilibria using the distance function related to the surface heat flux. Figure a represents the time series of the distance of the actual state of the ocean to the spin-up state and figure b represents the difference in distance between the actual state of the ocean and the spin-up state on one side and the unstable equilibria on the other side.

where S_i and S_{ieq} are the salinity in a grid point of the actual state of the ocean and in the equilibrium point, N the total number of grid points and M the number of surface boxes. The salinity distribution of the ocean adapts itself more rapidly to variations in the system than the meridional overturning function, but slower than the surface heat flux. In the top layer of the ocean the freshwater flux is directly influencing the salinity distribution of the ocean. In this layer variations in the salinity distribution will therefore be quite large and change rapidly. This might result in the same problem as with the surface heat flux. Therefore the salinity distribution of the top layer is omitted in the distance function. The result is shown in figure 4.11.

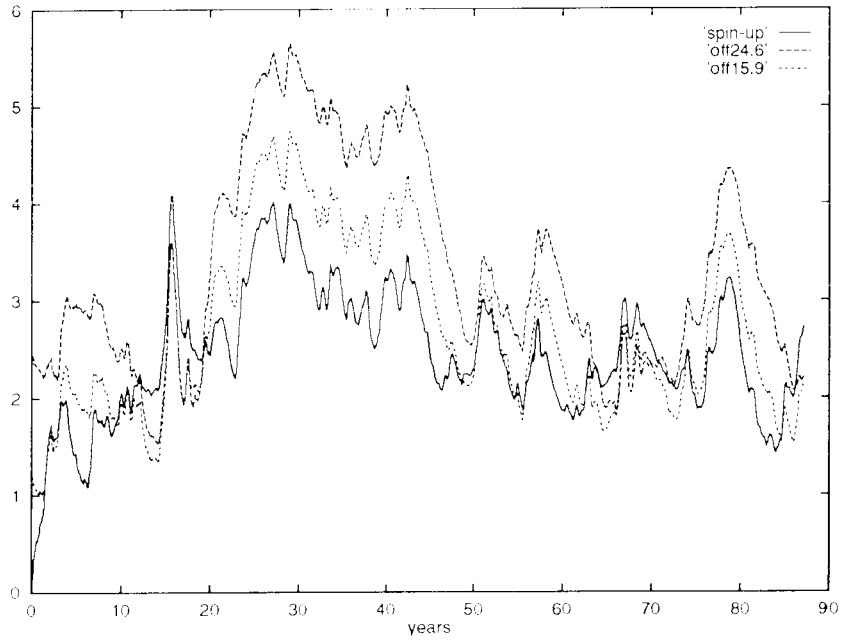

Figure 4.11: Time series of the distance to the equilibria using the distance function related to the salinity distribution of the ocean.

Again after about 15 years the distance of state of the ocean to the unstable equilibria is less than the distance to the spin-up state. The distance of the actual state of the system to the unstable equilibria soon afterwards indeed starts to increase, but still remains less than the distance between the system's state and the spin-up state for several years. This behaviour is in accordance with the previous described theory. After about 70 years

however the state of the system again is closer to the unstable equilibrium and remains so for a larger period. It seems however, that soon after this point another oscillation in the meridional heat transport takes place (see figure 4.8).

This distance function is reasonably able to represent the expected behaviour of the system if the unstable equilibria are important for the dynamical behaviour of the system. This result could therefore support the theory that the unstable equilibria are important for the dynamical behaviour of the system. It remains however still unclear whether this distance function is indeed able to represent the dynamical behaviour of the system properly. It is therefore not possible to conclude that there are indeed unstable equilibria which are important for the dynamical behaviour of the system. In the previous section we established however that a phase space description with at least one unstable equilibrium is the most likely and the results in this section are not in contradiction with this theory.

Chapter 5

Physical principles

In the previous chapter we tried to explain the oscillating behaviour of the system under a stochastic perturbation of the freshwater flux through a phase space description. The physical processes, which are important for this kind of behaviour remained however unclear. In this chapter the main objective will be to explain the oscillating behaviour of the ocean from a physical point of view. Are there sensitive areas in the ocean? What processes are important for the oscillating behaviour? Where does the time scale of about a century arise from? To answer these questions will be the main goal of this chapter.

5.1 Sensitive areas

A stochastic perturbation of the freshwater flux results in an oscillating behaviour of the system. This stochastic perturbation has a spatial structure, which covers the total ocean-basin. In order to investigate the possibility of sensitive areas in the ocean-basin it is interesting to restrict the stochastic perturbation to parts of the ocean and examine the differences in response. Therefore the following experiment was performed. First the model was integrated for about 2500 years with a stochastic perturbation of the freshwater flux over the whole basin. The standard deviation of the forcing was 40 % of the original maximum of the freshwater flux (see section 3.5). All other boundary conditions are the same as in the spin up experiment. Then this experiment was repeated with the stochastic forcing only applied to the upper half of the basin (from y=M/2 to y=M). The strength of the forcing was left unchanged. Also the experiment with the stochastic forcing only

applied to the lower half of the basin (from y=0 to y=M/2) was performed. The results are shown in figure 5.1.

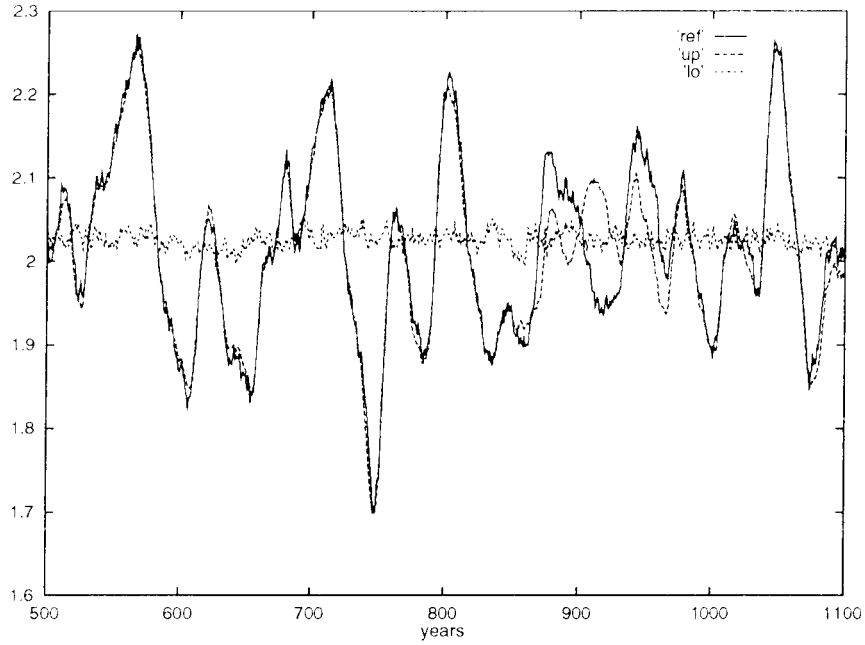

Figure 5.1: Meridional heat transport in 10^{14} W of the integration with a stochastic perturbation, which covers the total basin (solid line), only the upper half (dashed line, up) and only the lower half (dashed line, lo).

By examining figure 5.1 it appears, that the sensitive areas of the ocean are located in the upper half of the basin. The behaviour of the system in the cases, when the stochastic perturbation covers the total basin (total case) and when it covers only the upper half, is (upper case) almost identical. The difference in responses is very small. This is not only perceptible in the meridional heat transport, but also in several other quantities. If the stochastic perturbation is limited to the lower half of the ocean the response is very weak. The maximum deviation of the meridional heat transport from its equilibrium state is in the order of 1.5 %. The lower half of the ocean seems not to be sensitive to a stochastic perturbation of the freshwater flux. If we look at the time series of the upper and total case the most striking event happens after about 850 years of integration. Up until this point the system's behaviour in the upper and total case was nearly identical. Then suddenly the response of the system to the stochastic perturbation becomes

substantially different in these two cases. In the total case the stochastic perturbation also covers the lower half of the basin. Probably the external forcing in this region generated a perturbation in the ocean, which with the aid of the stochastic perturbation in the upper half of the basin was able to influence to behaviour of the system. This could explain the splitting up of the two time series. In both cases the system's behaviour still displays an oscillating character, but the period seems to be different in each case. The oscillations are at the year 910 even half a period out of phase. The most surprising event however is the reunification of the two time series after about 975 years. The response of the system to the stochastic forcing in the two cases was substantially different during a period of about 100 years, but then again becomes identical. It is possible that the stochastic forcing has triggered a process in the ocean with a period of about 100 years, which determines the long term behaviour of the system and seems to be quite persistent.

What is however the influence of the external forcing on this process ? After 910 years of integration the system's behaviour of the total and upper case seems to be half a period out of phase. When the stochastic perturbation is left on during the whole integration, the time series of these two cases reunite after another 65 years. It would be interesting to check whether this reunification of the two time series also takes place, when the stochastic perturbation is switched off after 910 years. In order to investigate this the above described experiments, when the stochastic perturbation covered the total and only the upper half of the basin, are repeated and after 910 years of integration the external forcing is switched off. The result is shown in figure 5.2.

The reunification of the two time series does not take place. The times series of the different cases remain substantially different. In contrast to the previous experiment this result does not support the theory of an internal process in the ocean, which determines the long term behaviour of the model. This experiment suggests, that there is no such process at all or at least that such a process is not able to survive without the aid of the stochastic perturbation. The influence of the external forcing on the reunification of the two time series in the previous experiment seems still to be considerable. This makes the explanation of the reunification quite difficult. It possible that there is an internal process, which determines the long term behaviour of the system, but it could also have a different explanation. This will be further investigated in the remainder of this chapter.

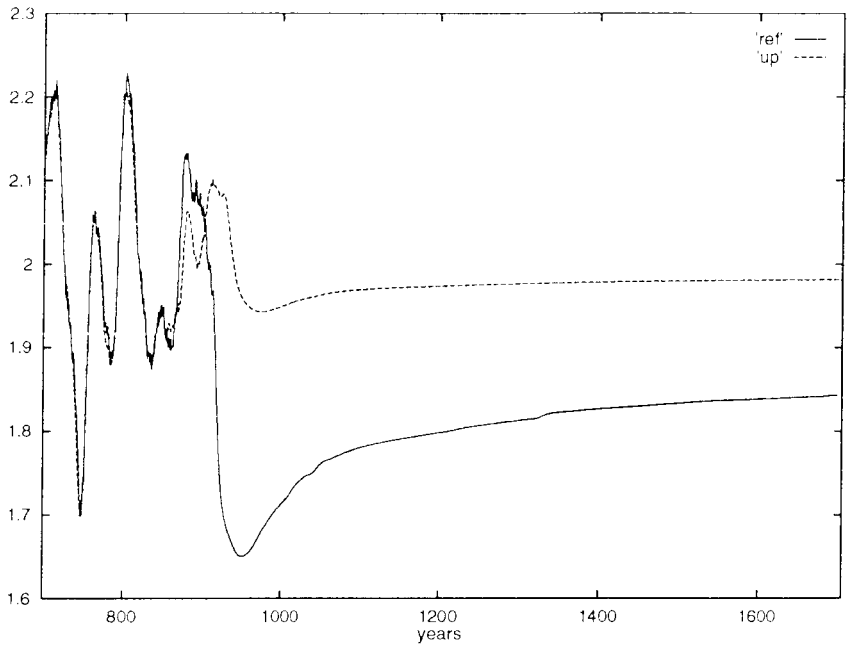

Figure 5.2: Time series of the meridional heat transport in 10^{14} W at y=M/2, when the stochastic perturbation, covering the whole surface (solid line) and only the top half (dashed line) of the basin, was switched off after 910 years.

5.1.1 Sensitive areas and convection

The most sensitive areas of the ocean are thus located in the upper half of the basin. This is also the area, where the process of deep water formation (convection) takes place. To test whether the variability in the system's behaviour is linked to variations in the process of deep water formation one oscillation is studied in detail. This is the same oscillation as described in section 4.2. The results are shown in figure 5.3 and 5.4.

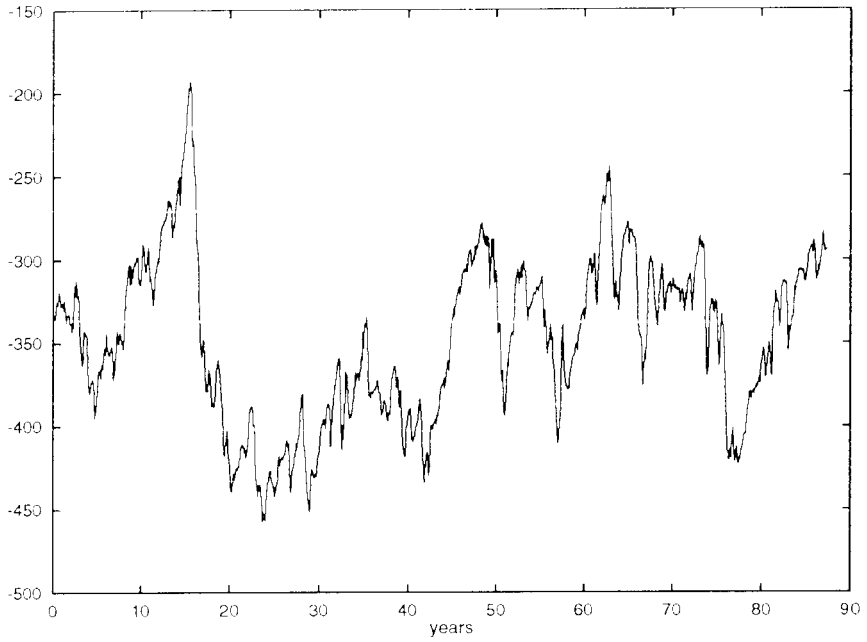

Figure 5.3: Time series of the total net ocean-atmosphere heat exchange in the convective area in 10^{12} W. The sign of the heat exchange is negative, because the ocean loses heat to the atmosphere.

The time series of the total net heat (figure 5.3), which is exchanged with the atmosphere in the area of deep water formation, shows substantially variability. After an initial increase of the total amount of heat exchange it decreases dramatically. This decrease is due to a decrease in the area, where deep water formation is taking place. The process of deep water formation is an important process for the heat balance of the ocean. The magnitude of the heat exchange between the ocean and atmosphere is determined by the difference between the sea surface temperature and the atmospheric temper-

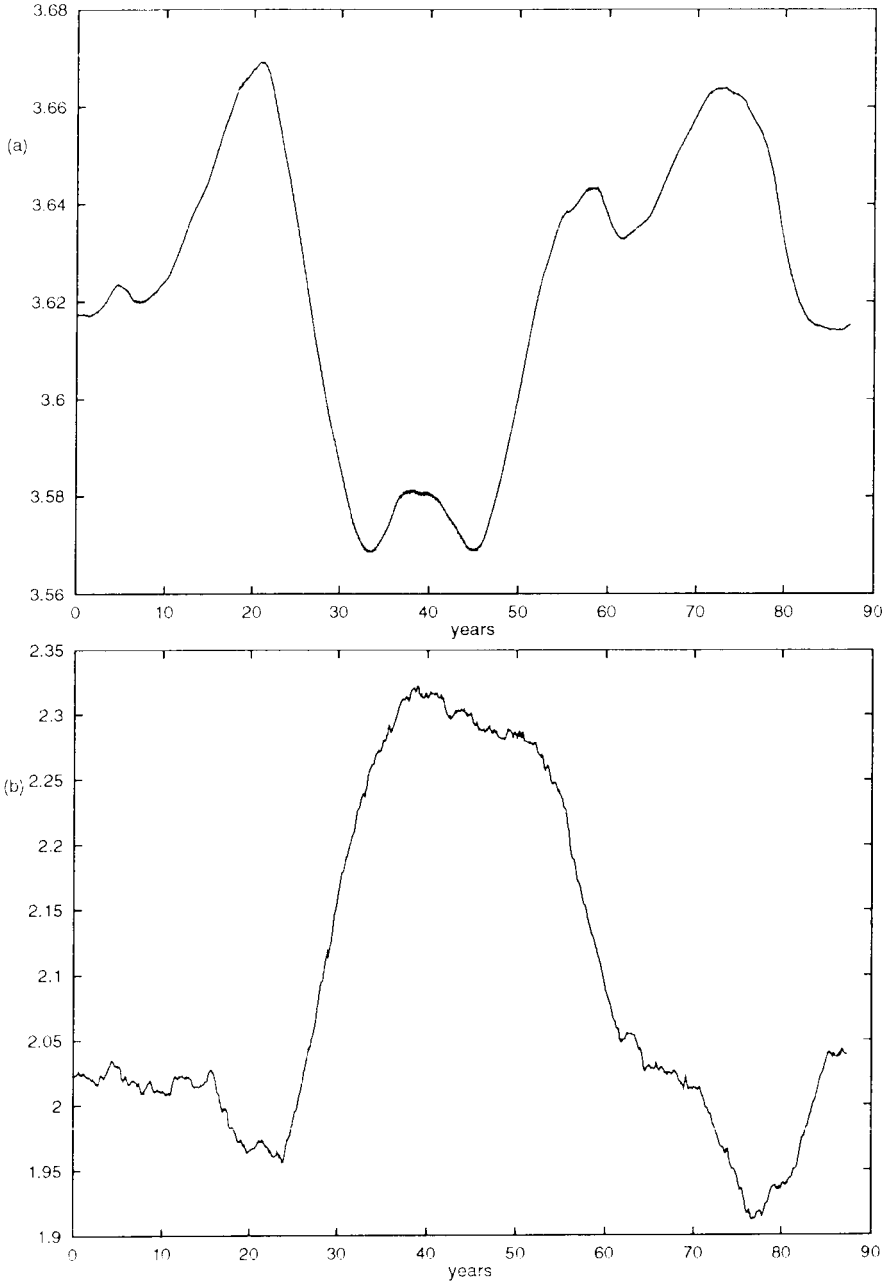

Figure 5.4: Time series of the mean temperature of the part of the deepest layer from y = 3M/4 to y = M in °C (figure a) and the meridional heat transport in 10^{14}W at y=M/2 (figure b).

ature. Through deep water formation relatively warm deep oceanic water is mixed to the surface, thereby enlarging the difference between the sea surface and atmospheric temperature. This results in an increase of the ocean-atmosphere heat exchange in the area, where deep water formation is taking place. The heat loss of the ocean in this area is therefore much larger than in areas, where no convection occurs. Variations in the size of the convective area therefore substantially influence the total ocean-atmosphere heat exchange. By reducing the size of the convective area less cold surface water is mixed downwards, thereby increasing the temperature of the deep ocean in the top quarter of the basin (figure 5.4a). At the bottom of the ocean deep oceanic water is advected equatorward. Increasing the temperature of the deep ocean therefore results in an increase of the total heat, which is transported equatorwards. Decreasing the convective area also results in a slowing down of the meridional overturning, thereby decreasing the heat transport from equator to pole along the surface. These effects combined result then in a decrease of the total meridional heat transport (figure 5.4b) as defined in section 3.3.

After about 15 years the total net ocean-atmosphere heat exchange in the convective area (figure 5.3) increases rapidly. This is due to an enlargement of the area, where convection is taking place. This results in a decrease of the temperature of the deep ocean in the top quarter of the basin (figure 5.4a) and in an increase of the meridional heat transport (figure 5.4b). From this we may conclude that variations in the process of deep water formation are indeed an important factor for the variability in the behaviour of the model.

The variability in the ocean-atmosphere heat exchange in the convective area is larger than the variability in the time series of the meridional heat transport. The large fluctuations in the time series of ocean-atmosphere heat exchange are easy to link to variations in the time series of the meridional heat transport. Small and rapid fluctuations in the time series of the ocean-atmosphere heat exchange are however not visible in the time series of the meridional heat transport. If the ocean-atmosphere heat exchange is relatively high or low during a longer period, the influence on the meridional heat transport is however easy perceptible. From about 45 until 70 years the ocean-atmosphere heat exchange is fluctuating around a relatively low value. During this period the meridional heat transport decreases substantially, which was to be expected. The meridional heat transport seems to react to the mean signal of the ocean-atmosphere heat exchange in the convective area.

5.1.2 Analysis

The time series of the ocean-atmosphere total net heat exchange in the convective area (figure 5.3) shows substantial variability. This time series contains small fluctuations, but also large jumps. Apparently the influence of the external forcing is at some points larger than at other points. In order to determine the sensitivity of the model at a given state, it would be useful, when the possible changes in this heat exchange could be estimated in advance. For this purpose the Convective Sensitive Area (CSA) analysis, which is developed by Lenderink and Haarsma [11], is tested. They demonstrated that for certain grid points the convective state as well as the non-convective state is possible. This possibility of multiple steady states is due to the formulation of mixed boundary conditions, i.e. the relaxation of the surface temperature to the atmospheric temperature and the prescribed freshwater flux, together with the vastly different time scales for the temperature forcing (short) and the salinity forcing (long). In the polar areas cold fresh surface water is located on top of warm saline bottom water. If in a stable situation by some perturbation mixing between the surface and deeper layers occurs, the surface layer becomes warmer and more saline. The increased heat in the surface layer is quickly released to the atmosphere. This results in a surface layer, which has the same temperature but is now more saline and thus denser than before the perturbation. In certain grid points the increased instability will sustain the convection. By investigating for non-convective grid points whether the convective state is also possible and vice versa an indication whether changes in the size or intensity of convection are likely to occur and an estimation of the possible gain or loss in total net heat exchange between ocean and atmosphere is obtained. To investigate whether convection can easily be triggered or suppressed a vertical column in the ocean is considered. This vertical column consists of 12 grid boxes stacked on top of each other. In the analysis it is assumed, that this column is surrounded by an ocean, which has stationary temperature, salinity and velocity distributions. These distributions are of course obtained from the state of the ocean, which is being analyzed.

A salinity perturbation is then applied to the surface box of the vertical column. This perturbation is large enough to trigger convection in most non-convective columns and to suppress convection in convective columns. The vertical column is then integrated, while keeping the surrounding ocean constant, for about half a year to reach a steady state. This integration is similar to the time integration of the complete model. Horizontal advec-

tion and diffusion in the column are however computed using the stationary distributions of the surrounding ocean, whereas vertical advection, diffusion and convection are computed using the salinity and temperature distributions inside the column. The difference between the state at the end of the integration and the actual state of the ocean is being analyzed. This procedure is repeated until all vertical columns of the ocean are analyzed.

In order to test this analysis the model is integrated from the spin-up state for 500 years. A stochastic perturbation is added to freshwater flux with a standard deviation of 0.4 times the original maximum of the freshwater flux (see section 3.5). All other boundary conditions are the same as in the spin-up experiment (see section 3.4). The analysis is performed during the integration after each model step. The analysis will of course not be able to predict all small fluctuations in the time series of the ocean-atmosphere total net heat exchange. It should however be able to estimate the trend in the changes of the ocean-atmosphere total net heat exchange in the convective area to be useful at all. Therefore time series of the moving average of the total net heat exchange in the convective area and of the by the analysis estimated possible changes in this heat exchange are made. The averaging time is chosen to be approximately 8 years. The results are shown in figure 5.5 and 5.6.

After about 25 years there is a reasonable increase of the total net heat, which is exchanged between ocean and atmosphere (figure 5.5). The possibility of this increase is fairly well predicted by the analysis, i.e. the time series of the potential additional heat exchange (figure 5.6a) estimates a large possible increase. Also after about 200, 260, 350 and 470 years a substantial increase of the total net heat exchange is noticeable Again the possibility of these jumps is reasonably predicted by the analysis. The time series of the potential additional heat exchange however contains more peaks. It indicates, that at other times also a reasonably large increase of the total net heat exchange can occur. These jumps are not present in the time series of the total net heat exchange. Probably the influence of the external forcing at that time prevented a large increase of the total net heat exchange. By closer examining figure 5.5 we see, that also after about 100, 370 and 430 years a considerable increase of the total net heat exchange takes place. The possibility of these jumps is not really predicted by the analysis, i.e. the increase of the total net heat exchange is seriously underestimated. Especially the jump after about 100 years is underestimated by a factor 2. Nevertheless the analysis seems to give an indication of the possible increase of the total heat exchange at a given state.

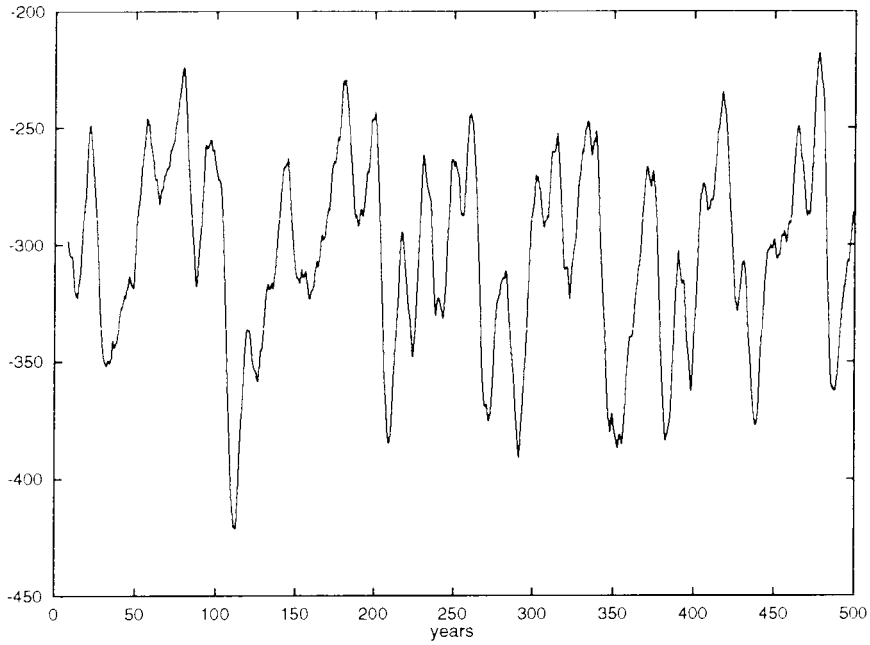

Figure 5.5: Time series of the moving average of the total net ocean-atmosphere heat exchange in the convective area in 10^{12} W. The sign of the heat exchange is negative, because the ocean loses heat to the atmosphere.

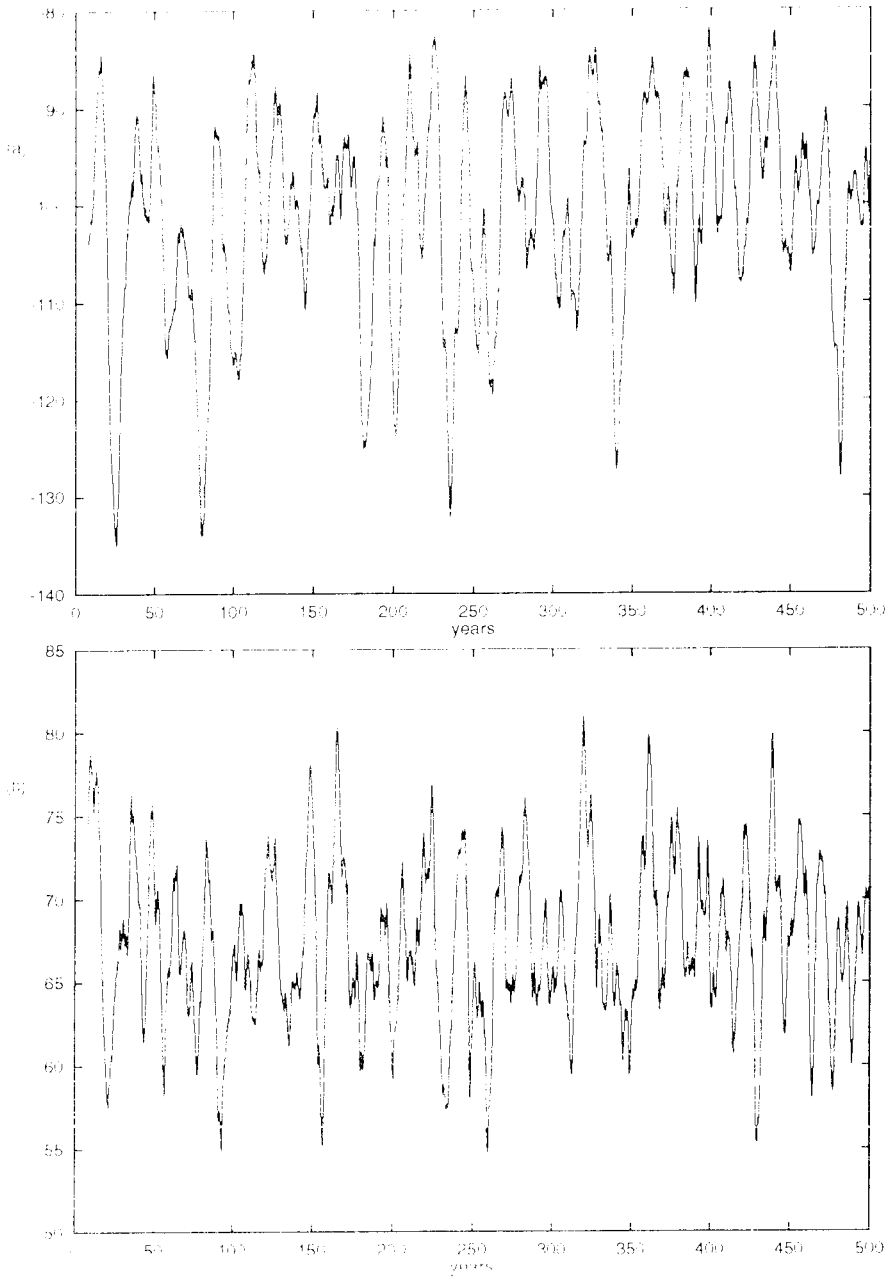

Figure 5.6: Time series of the moving average of the potential increase (figure a) and decrease (figure b) of the total net ocean-atmosphere heat exchange in the convective area in 10^{12} W.

In order to investigate the value of this analysis in more detail the cross correlation between the time series of the moving average of the total ocean-atmosphere heat exchange in the convective area and the moving average of the potential increase in this heat exchange is therefore calculated. The cross correlation of two time series x and y is defined as

$$R = \sum_{t=1}^{n} \frac{(x_t - \bar{x}) \cdot (y_t - \bar{y})}{n\delta_x\delta_y}, \tag{5.1}$$

where $\delta_x(\delta_y)$ is the standard deviation and $\bar{x}(\bar{y})$ the mean of the time series x(y). The cross correlation of the two time series is -0.5717. There is a fairly strong anti-correlation between the two time series. This indicates that a growth in the size or intensity of convection, thereby increasing the total net heat exchange between atmosphere and ocean in the convective area, results in a decrease of the potential additional heat exchange and vice versa. As shown before the magnitude of these variations in the two time series can differ substantially. The analysis underestimates the potential additional heat exchange sometimes considerably, but an increase of the total net heat exchange seems to result in a decrease of the potential additional heat exchange and vice versa. One expects therefore that the cross correlation of the derivatives of the two time series is fairly large. The cross correlation between the derivatives is 0.8425 which is in accordance with expectations.

The time series of the potential decrease in the total heat exchange (figure 5.6b) shows substantial variability. There are however no large peaks in the time series and so the decrease of the total net heat exchange is mostly underestimated. For example after about 100, 300 and 350 years there are substantial decreases in the total net heat exchange. These decreases are underestimated by a factor 2 by the analysis. The possible decrease of the total net heat exchange at a given state is not very well predicted by the analysis. In order to investigate the value of this analysis in more detail the cross correlation between the time series of the moving average of the total ocean-atmosphere heat exchange in the convective area and the moving average of the potential decrease in this heat exchange is calculated. The cross correlation is -0.2863 and so not very strong. One expects again that a decrease in the total net heat exchange should result in a decrease of the potential decrease in this heat exchange. To check this the cross correlation of the derivatives of the two time series is again computed. The cross correlation is -0.9126 and and thus fairly large. This result is in accordance with our expectations. The analysis seems reasonably able to predict the

potential additional heat exchange at a given state, whereas the potential decrease in this heat exchange is not very well predicted.

5.1.3 Freshwater flux and convection

Under a stochastic perturbation of the freshwater flux the system's behaviour displays substantially variability. In section 5.1.1 it was established, that changes in the size or intensity of the process of deep water formation are an important factor for this variability. In order to investigate, what the influence of the stochastic perturbation is onto this process, the experiment performed in section 5.1.1 was repeated. All boundary conditions and parameters are left unchanged. A time series of the stochastic component of the freshwater flux, averaged over the top quarter of the basin (from y=0.75M to y=M), is made. One expects that, the influence of the stochastic perturbation of the freshwater flux onto the process of deep water formation will only be noticeable, if there is additional precipitation or evaporation during a longer period. In order to filter the high frequency fluctuations a time series of the moving average of the stochastic component of the freshwater flux is made. The averaging time is chosen to be approximately 4 years. The result is shown in figure 5.7.

After 10 years we see, that moving average of the stochastic component of the freshwater flux in the top quarter of the basin increases substantially and is positive during a longer period. This means, that during a longer period there is additional precipitation in the top quarter of the basin. By again looking at figure 5.3 we see, that at the same time the ocean-atmosphere heat exchange in the convective area decreases substantially. Through additional precipitation in the top quarter of the basin the surface water in this region becomes less saline. This results in a decrease of the density of the surface water, thereby creating a more stable stratification. Additional precipitation in the top quarter of the basin thus suppresses the process of deep water formation. Less deep oceanic warm water is mixed to the surface, thereby decreasing the ocean-atmosphere heat exchange in the convective area.

After about 15 years the moving average decreases rapidly and becomes negative for a longer period (about 13 years). This means, that during this period, there is net evaporation in the top quarter of the basin. This of course has the opposite effect and results in an increase of the ocean-atmosphere heat exchange (figure 5.3). This relationship between the two time series is perceptible during the whole integration. A substantial increase (decrease) of the moving average immediately results in a decrease

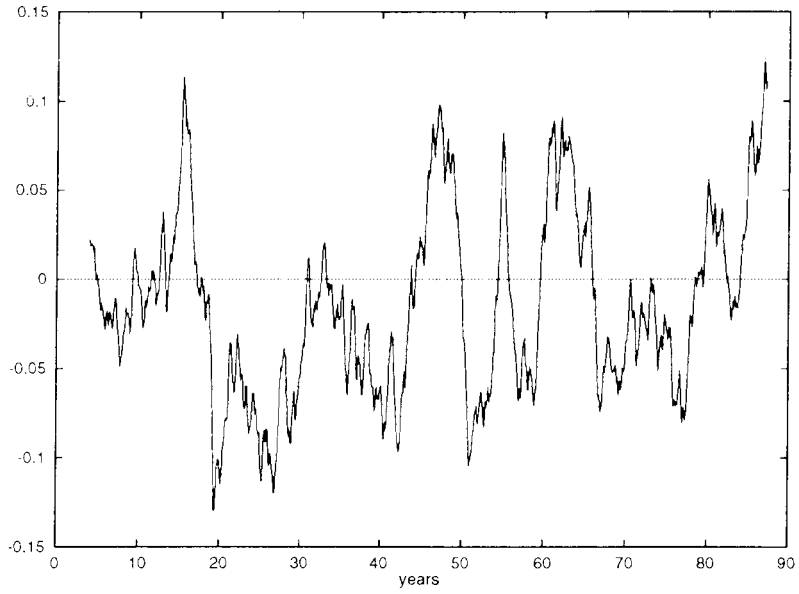

Figure 5.7: Time series of the moving average of the freshwater flux, averaged over the top quarter of the basin in m/year.

(increase) of the heat exchange in the convective area. Most fluctuations in the heat exchange can be linked to fluctuations in the moving average of the stochastic perturbation. The influence of the low frequency part of the stochastic component of the freshwater flux onto the process of deep water formation seems to be fairly strong. In order to investigate how strong this influence of the stochastic perturbation is the cross correlation of the two time series is calculated. The cross correlation of the two time series is 0.7174. There is a fairly strong correlation between the low frequency part of the stochastic perturbation of the freshwater flux and the variability in the process of deep water formation. This strong sensitivity to the low frequency signal of the freshwater forcing also explains the limited relevance of the potential convective areas. If convection is suppressed there will be a growth of potentially convective areas, thereby increasing the potential increase in ocean-atmospheric heat exchange in the convective area. Whether however additional convection is triggered in those potential convective areas strongly depends on the actual freshwater flux.

The influence of the low frequency part of the stochastic perturbation of the freshwater flux on variations in the process of deep water formation

on decadal time scales is fairly strong. There are however also variations in the process of deep water formation which have a longer time scale. One expects that these variations are determined by the internal dynamics of the system. In order to investigate this two longer time series of the moving average of the freshwater flux, averaged over the top quarter of the basin, and the heat exchange in the convective area are used. Those two time series are obtained from the experiment performed in section 5.1.2 and have a length of 500 years. The cross correlation between those time series is 0.4296. There is a substantial decrease in the cross correlation which one expects when variations in the process of deep water formation on longer time scales are indeed determined by the internal dynamics of the model.

5.2 Sensitivity to initial conditions

In the previous section it was established that fluctuations in the external forcing with time scales in the order of a decade strongly determine the dynamics of the system. In order to investigate how fast the system loses its memory about its initial state the model is integrated with the same forcing using three different initial conditions. If the effect of the external forcing depends on the state of the ocean the system's behaviour will be sensitive to different initial states. Therefore the model is integrated three times for about 400 years under a stochastic perturbation of the freshwater flux with a standard deviation of 0.4 times the maximum of the original freshwater flux. All other parameters and boundary conditions are the same as in the spin-up experiment (see 3.4). In each of the three integrations a different starting point is used. The first starting point is the spin-up state. The states of the ocean after 34.9 and 87.2 years integration are used as the two other starting points. The result is shown in figure 5.8. During the first 35 years the time series of the three different integrations show substantial differences. Afterwards the behaviour of the system is reasonably identical in all three cases. The three time series unify after about 100 years, yielding the conclusion that the system has lost all its memory with respect to the initial state after about 100 years. In the case where only one stable equilibrium is important for the dynamical behaviour of the system one could expect this kind of behaviour.

In chapter 4 however we established that is very likely that there are also unstable equilibria which are important for the dynamical behaviour of the system. This makes the explanation of the unification in this case

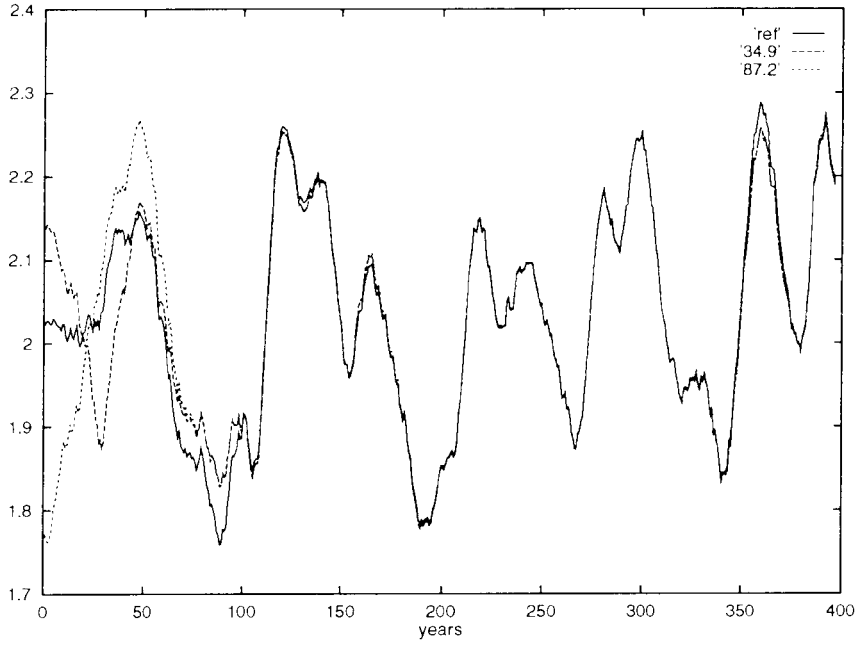

Figure 5.8: Time series of the meridional heat transport in 10^{14} W at y=M/2, when a stochastic perturbation is added to the freshwater flux, starting from three different initial states.

rather difficult. The external forcing is probably crucial for the dynamical behaviour of the system and determines whether the system moves towards an stable or an unstable equilibrium. In all three integrations the external forcing is identical, therefore after a period of time the system will therefore move, in all three integrations, towards the same stable equilibrium. If the system is close to an stable equilibrium the attraction force of this equilibrium becomes important. The system is drawn towards this equilibrium and the influence of the external forcing is needed to keep the system away from this equilibrium. In all three integrations the external forcing, which is need to balance the attraction force, is identical. It is therefore possible that under the influence of the attraction force the system is drawn in all three integrations to the same phase path.

The result of this experiment explains the outcome of the experiment performed in section 5.1. After about 125 years a reunification of the two time series in figure 5.1 took place. In this section we found, that the behaviour of the system is completely determined by the external forcing irrespective of the initial state of the ocean. The explanation of this reunification is now quite easy. The external forcing at the upper half of the basin in the upper and total case is identical during the whole integration. This means that, if the time series of the upper and total case become different at some point, they will reunite after a period of time.

The behaviour of the system is strongly determined by the external forcing. The system loses its memory about its initial condition after about 100 years. It appears that influence of the stochastic perturbation on the behaviour of the model is independent of the state of the ocean. In section 4.2 we found however that the influence of the external forcing on the system's behaviour is very well dependent on the actual state of the ocean. These results seem to contradict each other. It is however very well possible that the external forcing determines the direction in which the system moves in the phase space, but that the magnitude of its influence onto the system's behaviour depends on the actual state of the ocean. If the system is close to an stable equilibrium the influence will be smaller than when the system is close to an unstable equilibrium.

5.3 Time scale

The period after which the reunification takes place is in the order of about 100 years. This time scale seems also to be a characteristic period of the

system. The existence of this time scale has not been yet explained. By again examining figure 5.4 we see, that the oscillating behaviour of the system with a time scale of about 100 years is not only visible in the meridional heat transport, but also in the temperature of the deep ocean. After an initial increase of the temperature of the deep ocean during the first 20 years, it decreases rapidly with about 0.1 °C. During the next 50 years the temperature slowly increases again. Variations in the temperature of the deep ocean substantially influence the stability of the ocean-circulation. If the temperature of the deep ocean is increased, the density on the deep ocean decreases, thereby creating a less stable stratification of the ocean. An increase of the temperature of the deep ocean therefore favours the process of deep water formation. A decrease of this temperature has of course the opposite effect. From figure 5.4 it seems, that if the temperature of the ocean becomes larger than a certain threshold a jump in the meridional heat transport takes place. The characteristic time scale of the system seems to be related to variations in the temperature of the deep ocean. The size and intensity of the process of deep water formation determine the magnitude of ocean-atmosphere heat exchange in the convective area. Increasing this heat exchange will result in a decrease of the temperature of the deep ocean, whereas a decrease results in an increase of the temperature of the deep ocean (see section 5.1.1). This process shows however substantially variability on short time scales and it seems unlikely, that this will explain the characteristic time scale. There is however another process, which is important for the temperature of the deep ocean. At the equator the temperature of the deep ocean is about 0.15 °C higher than the temperature of the deep ocean at high latitudes. Through diffusion therefore heat is transported from equator to pole. The variations in the deep oceanic temperature are in the order of 0.1 °C. Using

$$\frac{\partial T}{\partial t} = \kappa_h \nabla_2^2 T \tag{5.2}$$

an estimation can be made of the time which is needed to increase the temperature of the deep ocean with this magnitude through diffusion. For a pole to equator distance of about $3.5\ 10^3$ km and a temperature difference of 0.15 °C, $\nabla_2^2 T$ is in the order of $1.22 \cdot 10^{-14}$ °C m^{-2}. Therefore the characteristic time for changes in the deep oceanic temperature in the order of 0.1°C is about

$$\tau = \frac{0.1}{\kappa_h \cdot 1.2210^{-14} \cdot \text{seconds per year}} \approx 80\text{years}. \tag{5.3}$$

This time is in the order of magnitude of the characteristic period, which was found in the system's behaviour. The characteristic period of the system is probably determined by the process of diffusion. In order to test whether the process of diffusion indeed determines the characteristic time scale of the system the horizontal diffusion coefficient will be varied. A smaller diffusion coefficient will result in an increase of the characteristic period. The characteristic period of the system will namely be determined by the process, which is important for the behaviour of the system, with the longest time scale. Enlarging the diffusion coefficient on the other hand does not necessarily imply, that the characteristic period of the system will decrease. By enlarging the diffusion coefficient it could be, that other processes, which now will have the longest time scale, will determine the characteristic period.

The horizontal diffusion coefficient is therefore decreased by a factor 5, while all other parameters and boundary conditions are the same as in the spin-up experiment (see section 3.4). The model was then integrated for about 2500 years to reach an equilibrium state. The system did however not converge to an equilibrium state (see figure 5.9). The system's behaviour

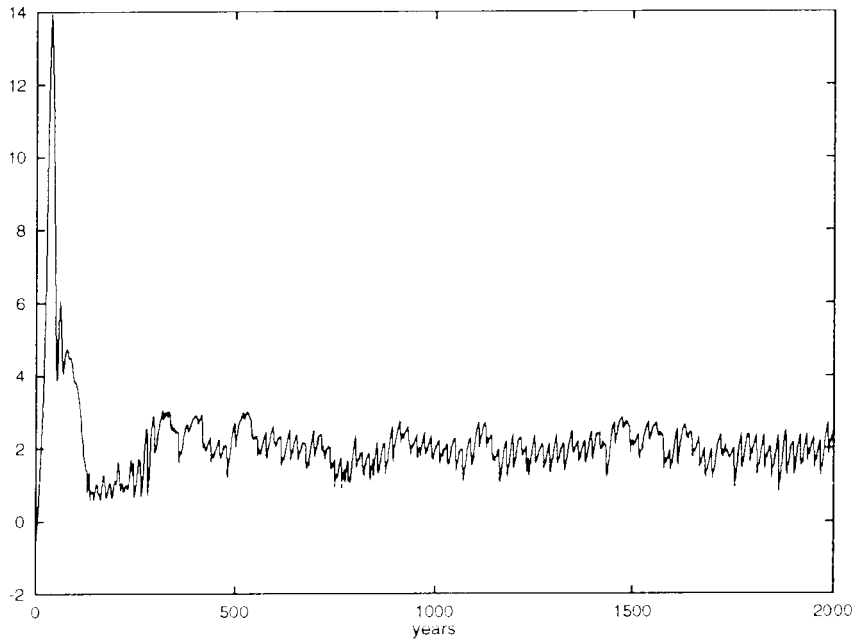

Figure 5.9: Time series of the meridional heat transport in 10^{14} W at y=M/2 using a diffusion coefficient of $0.6 \cdot 10^3$.

displayed spontaneous, substantial variability. To examine the influence of the diffusion coefficient on the characteristic period of the system is thus not possible with this experiment.

Several other values for the horizontal diffusion coefficient are tried, but a reasonable decrease of the horizontal diffusion coefficient always implies, that the system does not converge to an equilibrium. If the horizontal diffusion coefficient is decreased by a factor 2, the system still does not converge to an equilibrium state, but the spontaneous variability remains limited (see figure 5.10). Only during the first years there is substantial variability. After about 400 years there is only a trend visible in the meridional heat transport.

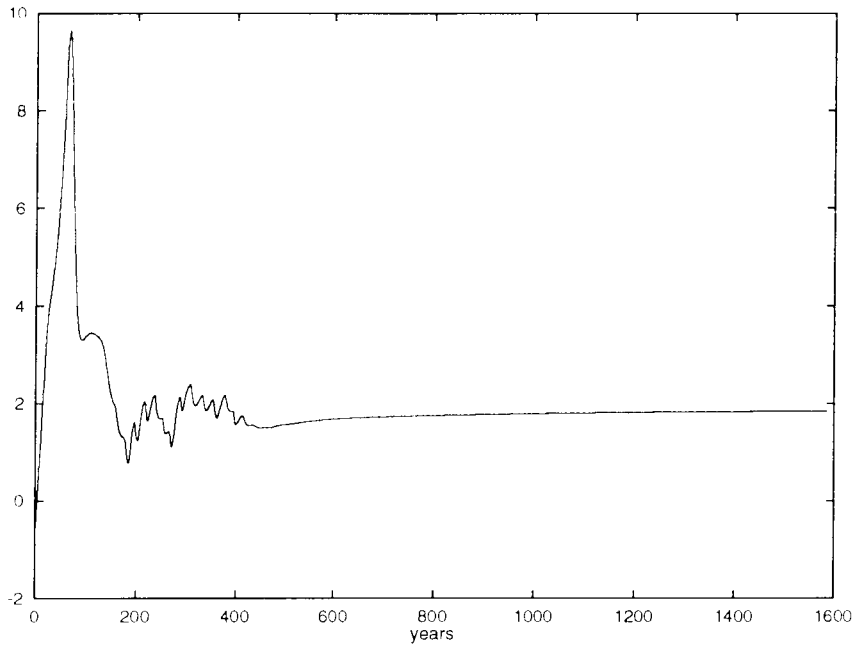

Figure 5.10: Time series of the meridional heat transport in 10^{14} W at y=M/2 using a diffusion coefficient of $1.5 \cdot 10^3$.

Although the system does not converge to an equilibrium, a stochastic perturbation with a standard deviation of 0.4 times the original maximum of the freshwater flux (see section 3.5) is added to the freshwater flux after 1600 years of integration. The model is then integrated for another 3500 years, while all other parameters and boundary conditions are left unchanged. The result is shown in figure 5.11.

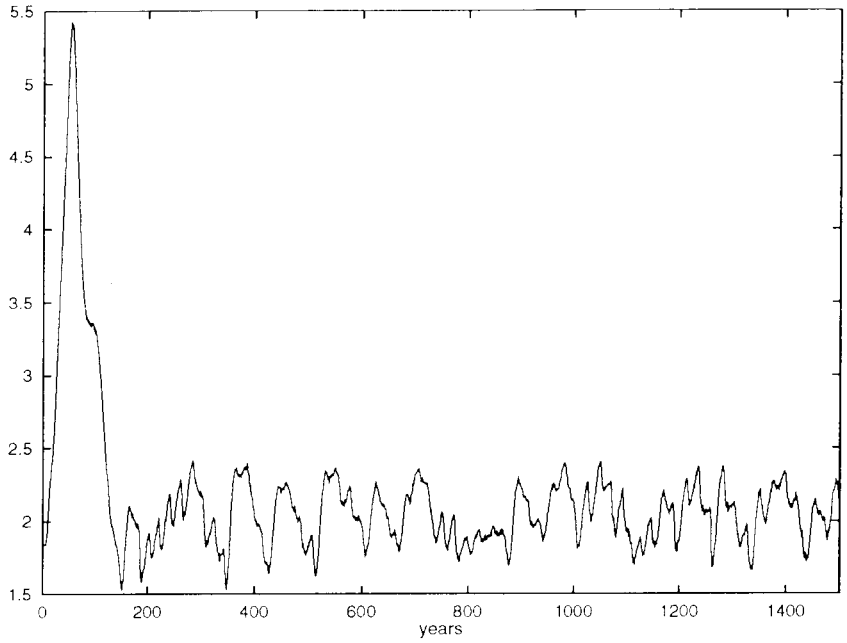

Figure 5.11: Time series of the meridional heat transport in 10^{14} W at y=M/2 using a diffusion coefficient of $1.5 \cdot 10^3$ under a stochastic perturbation of the freshwater flux.

The time series of the meridional heat transport displays a very large jump at the beginning of the integration. After about 200 years the system displays the same oscillating character as found in the previous performed experiments (see section 3.6). The difference between the maximum and the minimum value of the meridional heat transport however seems to be larger. In order to determine the characteristic period of the system the first 200 years of the time series are neglected and of the remaining part a power spectrum is made. The result is shown in figure 5.12. The characteristic

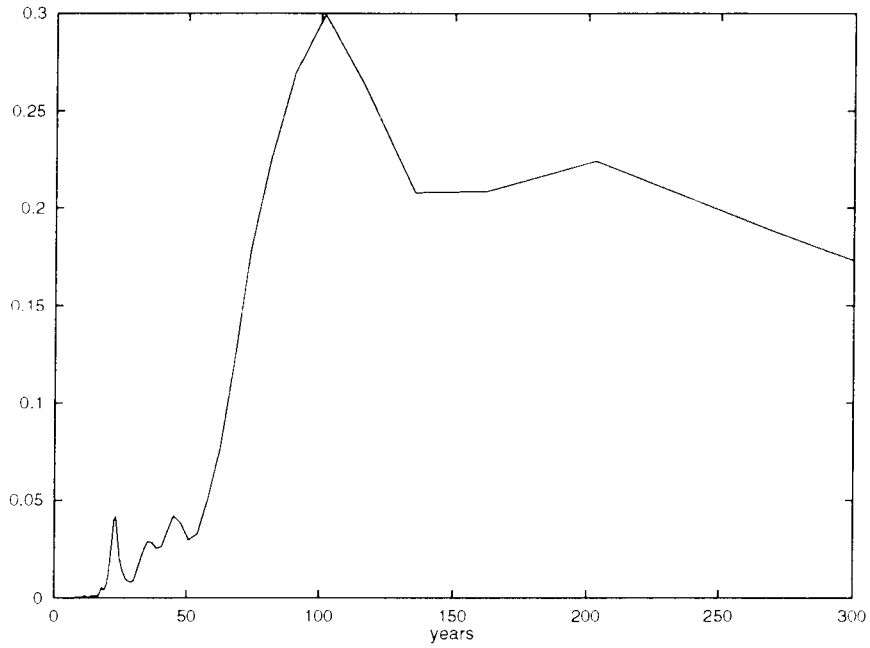

Figure 5.12: Power spectrum of the meridional heat transport. The multiplying limits for the 95 % confidence interval are 0.598 and 2.00.

period of the system is in the order of 100 years. By decreasing the horizontal diffusion coefficient the characteristic time scale of the system did not substantially increase. We therefore cannot conclude, that the characteristic time scale is determined by the horizontal diffusion coefficient. It is however possible that by decreasing the horizontal diffusion coefficient, the properties of the system change substantially. Therefore we also cannot conclude, that the horizontal diffusion coefficient does not determine the characteristic time scale of the system. Additional experiments should be performed to further investigate this. Probably a budget analysis of all terms, which are

responsible for the variations of the temperature of the deep ocean will give some answers. Due to lack of time this experiment is however not performed here.

Chapter 6

Conclusion

The internal variability in an ocean circulation model has been investigated. The model consists of a rectangular basin, which represents the North Atlantic ocean. The influence of bottom topography and the curvature of the earth has not been taken into account. This model only contains an oceanic component and the influence of the atmosphere onto the ocean is described through boundary conditions. The heat exchange between ocean and atmosphere is described through linear relaxation of the sea surface temperature to a prescribed temperature distribution, which remains constant in time. The wind stress and freshwater flux are also assumed to be constant in time and only spatial variations are taken into account. The ocean circulation reasonably resembles the circulation in the North Atlantic, despite a somewhat weak meridional heat transport.

A stochastic component was added to the freshwater flux. Under this stochastic perturbation of the freshwater flux the ocean circulation displayed substantially variability. The system's behaviour showed an oscillating character with a characteristic period in the order of about 100 years. In chapter 2 a theory about simple stochastic climate models was described. This theory is unable to explain the dynamical behaviour of the ocean model with preferred time scales. The theory predicts that the natural variability of the ocean circulation takes place on all possible time scales.

Analysis of the dynamical behaviour of the ocean model suggests that a phase space description with a stable and at least one unstable equilibrium is the most likely description. Although the numerical search for an unstable equilibrium of the ocean system did not succeed, it was reasonably well established that there is at least one unstable equilibrium, which is impor-

tant for the dynamical behaviour of the model. The existence of multiple steady equilibria in a simple general ocean circulation model has already been established by several authors (see [10], [12], [13] and [19]). That, apparently, unstable equilibria of the ocean system are also important for its dynamical behaviour was however not very well recognized.

The physical principles, which are important for the variability of the ocean were studied in detail in chapter 5. The most important physical process for the variability in the ocean circulation seems to be the process of deep water formation (convection). This process takes place in the polar area. In this area the effect of cooling of the sea surface temperature is larger than the effect of precipitation, thereby creating a relatively high surface density. This results in an unstable stratification of the ocean and so relatively warm, saline deep oceanic water is mixed to the surface. This process is also present in the real Atlantic ocean and is called the process of North Atlantic deep water (NADW) formation.

The influence of the stochastic perturbation of the freshwater flux on the variability in the process of deep water formation is rather large. Additional precipitation in the area, where convection is taking place, results in a less saline surface distribution in this area. This result in a decrease of the density of the the surface water, thereby creating a more stable stratification in the ocean. Additional precipitation results therefore in a decrease in size and intensity of the process of deep water formation. Additional evaporation has of course the opposite effect. An analysis predicting the sensitivity of the ocean to the stochastic perturbation of the freshwater flux was tested in chapter 5. This analysis was reasonably able to predict the increases in the size and intensity of the process of deep water formation, but the decreases were rather poorly predicted.

The influence of the stochastic component of the freshwater flux on the behaviour of the model, especially at decadal time scales, appeared however to be very strong. On longer time scales the internal dynamics of the ocean becomes more important. If the ocean model is integrated under a stochastic perturbation of the freshwater flux starting from different initial points, the behaviour of the system in the different integrations becomes almost equivalent after about 100 years. Apparently the behaviour of the system has lost its memory about its initial state after about 100 years. The influence of the stochastic perturbation on the dynamical behaviour of the system is rather strong, although the precise magnitude of this influence depends on the actual state of the ocean. This fairly strong dependence of the dynamical behaviour of the system on the stochastic perturbation of the freshwater flux

makes however describing the atmospheric influence onto the ocean through a stochastic perturbation not very realistic. Probably typical structures and seasonal variations in the atmospheric forcing, which are present in the real atmosphere, should be taken into account. It remains therefore uncertain whether the, in this report, found variability of the ocean circulation is also present when a more realistic description for the atmospheric influence onto the ocean is used.

The characteristic time scale of about 100 years in the oscillating behaviour of the model is still unexplained. This time scale seems to be related to variations in the temperature of the deep ocean in the top quarter of the basin. The temperature of the deep ocean slowly increases until a certain critical value and then drops again. The slow increase of this temperature seems to be related to horizontal diffusion of heat from the equator, whereas the rapid decrease in temperature is related to an increase in size and intensity of the process of deep water formation. A more detailed study however to investigate the reason for this variability in the temperature of the deep ocean is necessary.

ACKNOWLEDGEMENTS.

First of all I would like to thank professor Hermans of the Technical University Delft for giving me the opportunity to perform my graduate research at the KNMI in the Bilt, and for his support in my work. Further many thanks are due to all the members of the predictability group at KNMI. You created a very positive and pleasant working environment.

Among them a few should be mentioned in particular:

T.Opsteegh, head of the predictability group, for allowing me to stay for almost a year with his group, R.Pasmanter for his help and valuable advise during this research, N.Weber for her help in understanding the article of Hasselmann and being my supervisor during the first months of my stay, G.Lenderink for all his help and the many useful discussions we have had during this research and last, but certainly not least, R.Haarsma, who was my supervisor during the last months of my graduate research. Rein, I really enjoyed working with you. You were always very helpful, patient, enthusiastic and able to come up with creative new ideas and experiments.

Finally I would like to thank my parents and sister and all of my friends for their support and interest in my research.

Bibliography

[1] Gihman I.I.,Skorohod A.V. 1972 *Stochastic Differential equations* Springer-Verlag Berlin Heidelberg New York

[2] Hasselmann K. 1976 *Stochastic Climate Models Part I Theory* Tellus 28,6 page 473-485

[3] Hinze J.O. 1959 *Turbulence*, Mcgraw-Hill

[4] Holton J.R. *An introduction to Dynamic Meteorology* International geophysics series, volume 23, second ed., Academic Press

[5] Huang R.X. 1993 *Real freshwater flux as a natural boundary condition for the salinity balance and thermohaline circulation forced by evaporation and precipitation* J.P.O 23, page 2428-2446

[6] Jordan D.W. and Smith P. *Nonlinear ordinary differential equations* Oxford Ubiversity Press, New York, 1987 second ed.

[7] van Kampen N.G. 1976 *The expansion of the master equation* Adv. Chem. Phys. 34, page 245-309

[8] Kloeden P.E.,Platen E. and Schurz H. *Numerical solution of SDE through computer experiments*, Springer-Verlag 1994

[9] Lenderink G. *Sensitivity and internal variability of the Thermohaline Circulation*, Afstudeerverslag TU Delft, march 1992

[10] Lenderink G. and Haarsma R.J. 1994 *Variability and multiple equilibria of the thermohaline circulation associated with deep-water formation* J.P.O. 24, page 1480 -1493

[11] Lenderink G. and Haarsma R.J. 1995 *The influence of sea-ice on the variability of the thermohaline circulation*
in preparation

[12] Marotzke J. et al. 1988 *Instability and multiple steady states in a meridional-plane model of the thermohaline circulation*
Tellus 40A, page 162-172

[13] Mikolajewicz U. and E. Maier-Reimer 1990 *Internal secular variability in an ocean general circulation model*, Climate Dynamics 4, page 145-156

[14] Mysak L.A. et al. 1993 *Century-scale variability in a randomly forced, two-dimensional thermohaline ocean circulation model*
Climate Dynamics 8, page 103-116

[15] Nieuwstadt F.T.M. 1992 *Turbulentie*, epsilon uitgaven, Utrecht

[16] Peixoto J.P. and Oort A.H. 1993 *Physics of climate*
American Institute of Physics, third edition, New York

[17] Weaver A.J. and Sarachil E.S. 1991 *The role of mixed boundary conditions in numericals models of the ocean's climate*
J.P.O 21, page 1470-1493

[18] Weaver A.J. and Sarachik E.S. 1991 *Evidence for decadal variability in an ocean general circulation model: an advective mechanism*
Atmosphere-Ocean 29, page 197-231

[19] Weaver A.J. et al. 1993 *Stability and variability of the Thermohaline Circulation*, J.P.O 23, page 39-60

[20] Weisse R. et al. 1993 *Decadal variability of the north atlantic in an ocean general circulation model*
report 108, Max-Planck-Institut für meteorologie, Hamburg

Appendix A

Derivations of spectra and covariances

A.1 Linear case, $\tau_x \ll t \ll \tau_y$

Spectrum:

By writing

$$v_i'(t) = \int_{-\infty}^{\infty} V_i(\omega) \exp(i\omega t) d\omega \qquad \text{(A.1)}$$

the solution of equation (2.7) can be expressed as

$$\delta y_i'(t) = \int_{-\infty}^{\infty} Y_i(\omega) \exp(i\omega t) d\omega - \int_{-\infty}^{\infty} Y_i(\omega) d\omega \qquad \text{(A.2)}$$

$$\text{where} \quad Y_i(\omega) = \frac{V_i(\omega)}{i\omega} \quad (\omega \neq 0)$$

The second term on the right hand side of equation (A.2) arises through the initial condition on t=0.

Because v'(t) represents a stationary random process it follows that the Fourier components are statistically orthogonal, i.e.

$$\langle V_i(\omega) V_j^*(\omega') \rangle = \delta(\omega - \omega') F_{ij}(\omega) \qquad \text{(A.3)}$$

where $F_{ij}(\omega)$ denotes the cross spectrum of $v_i'(t)$ and $*$ denotes the complex conjugate.

It immediately follows that the Fourier components $Y_i(\omega)$ are then also statistically orthogonal and the cross spectrum of $\delta y_i'$(t) , $G_{ij}(\omega)$, is given

by

$$G_{ij}(\omega) = \frac{F_{ij}(\omega)}{\omega^2} \qquad (\omega \neq 0) \tag{A.4}$$

Covariance:

In order to calculate the covariance of $y_i'(t)$ we use (A.2) and (A.3) and we find

$$\begin{aligned} \langle \delta y_i'(t) \delta y_j'(t) \rangle &= \int_{-\infty}^{\infty} \frac{F_{ij}(\omega)}{\omega^2} (e^{i\omega t} e^{-i\omega t} - e^{i\omega t} - e^{-i\omega t} + 1) d\omega \\ &= 2 \int_{-\infty}^{\infty} \frac{F_{ij}(\omega)}{\omega^2} (1 - \cos(\omega t)) d\omega \end{aligned} \tag{A.5}$$

The function $\frac{1}{2\pi t} \frac{2(1-\cos(\omega t))}{\omega^2}$ can be approximated by a delta-function if t becomes large. The function has a maximum value of $\frac{t}{2\pi}$ at ω=0 and the term $\frac{1}{2\pi t}$ makes sure that the function approaches zero outside $\omega = 0$. The only thing we have to check, to be sure that we are doing a legal operation by replacing, is whether the integral of the function is equal to 1. Through partial integration this follows almost immediately.

$$\int_{-\infty}^{\infty} \frac{1}{2\pi t} \frac{2(1-\cos(\omega t))}{\omega^2} d\omega = \int_{-\infty}^{\infty} \frac{\sin(\omega t)}{\pi \omega} d\omega = 1 \tag{A.6}$$

For large t (still $t \ll \tau_y$) equation (A.5) therefore becomes

$$\langle y_i' y_j' \rangle = 2\pi t F_{ij}(0) \tag{A.7}$$

A.2 Linear feedback, t = O(τ_y)

Spectrum:

we are going to solve these equations in the Fourier domain and using

$$v_i'(t) = \int_{-\infty}^{\infty} U_i(\omega) \exp(i\omega t) d\omega$$

the solution of equation (2.13) can be expressed as

$$Y(\omega) = (i\omega I - V)^{-1} U(\omega) = TU(\omega) \tag{A.8}$$

The cross spectrum G_{ij} follows almost immediately by multiplying $Y(\omega)$ with its complex conjugate, thus $G_{ij} = T_{ik} T_{jl}^* F_{kl}(\omega)$. Here $F_{ij}(\omega)$ is again

the cross spectrum of $v_i'(t)$ and for large t we can replace $F_{ij}(\omega)$ by $F_{ij}(0)$ and so we finally get for the cross spectrum the following expression:

$$G_{ij}(\omega) = T_{ik}T_{jl}^{*}F_{kl}(0) \tag{A.9}$$

If the matrix V is a diagonal matrix with λ_i on the diagonal equation (A.9) reduces to:

$$G_{ij}(\omega) = \frac{F_{ij}(0)}{(\omega + i\lambda_i)(\omega - i\lambda_j)} \tag{A.10}$$

Covariance:

In order to calculate the covariance, $[y_i'(t)y_j'(t)] = [(y_i(t) - y_{i0})(y_j(t) - y_{j0})]$, we first define:

$$R_{ij}(t) = [(y_i(t) - [y_i(t)])(y_j(t) - [y_j(t)])] \tag{A.11}$$

Using equation 2.13 and the fact that $v_i'(t+\tau)$ and $y_j(t)$ are statistically uncorrelated for $\tau > 0$, since the correlation time scale of the random forcing is regarded as infinitely short compared with the correlation time scale of the response, we obtain the following differential equation

$$\begin{aligned}
\frac{dR_{ij}(t)}{dt} &= [\frac{d(y_i(t) - [y_i(t)])}{dt}(y_j(t) - [y_j(t)])] + \\
&\quad [(y_i(t) - [y_i(t)])\frac{d(y_j(t) - [y_j(t)])}{dt}] \\
&= [(V_{ik}y_k(t) + v_i'(t) - V_{ik}[y_k(t)])(y_j(t) - [y_j(t)])] + \\
&\quad [(y_i(t) - [y_i(t)])(V_{jk}y_k(t) + v_j'(t) - V_{jk}[y_k(t)])] \\
&= V_{ik}R_{kj} + R_{ik}V_{jk} + 2\pi F_{ij}(0)
\end{aligned} \tag{A.12}$$

and the solution is given by

$$R = R_\infty - e^{Vt}R_\infty e^{V^T t}, \tag{A.13}$$

where R_∞ denotes the asymptotic stationary solution of A.12. This is possible, because we have assumed that we have a stable equilibrium state.

We also define the covariance with lag τ :

$$\hat{S}_{ij}(t+\tau) = [(y_i(t+\tau) - [y_i(t+\tau)])(y_j(t) - [y_j(t)])] \tag{A.14}$$

Again using equation (2.13) and the fact that $v_i'(t+\tau)$ and $y_j(t)$ are statistically uncorrelated for $\tau > 0$, we obtain the following differential equation

$$\begin{aligned}
\frac{\partial \hat{S}_{ij}(t,\tau)}{\partial \tau} &= [\frac{\partial(y_i(t+\tau) - [y_i(t+\tau)])}{\partial \tau}(y_j(t) - [y_j(t)])] \\
&= [(V_{ik}y_k(t+\tau) + v_i'(t+\tau) - V_{ik}[y_k(t+\tau)])(y_j(t) - [y_j(t)])] \\
&= V_{ik}\hat{S}_{kj} \qquad (\tau > 0)
\end{aligned} \tag{A.15}$$

and the solution is given by

$$\hat{S}(t,\tau) \;=\; e^{V\tau}\hat{S}(t,0) \quad (\tau > 0). \tag{A.16}$$

We are especially interested in the asymptotic stationary solution, which can be compared with observed climatic time series. The asymptotic solution of A.16 is given by:

$$S(\tau) \;=\; \lim_{t\to\infty}\hat{S}(t,\tau) \;=\; e^{V\tau}R_\infty \quad (\tau > 0) \tag{A.17}$$

The derivation for $\tau < 0$ is equivalent and we find:

$$S(\tau) \;=\; \lim_{t\to\infty}\hat{S}(t,\tau) \;=\; R_\infty e^{-V^T\tau} \quad (\tau > 0) \tag{A.18}$$

The covariance $[y_i' y_j']$ can now be written as

$$[y_i' y_j'] \;=\; (S_{ij}(0) - S_{ij}(\tau)) + (S_{ji}(0) - S_{ji}(\tau)). \tag{A.19}$$

Appendix B

Fundamental equations

Momentum equation:

$$\frac{D\vec{u}}{Dt} + 2\Omega \times \vec{u} = -\frac{1}{\rho}\nabla_3 p - \vec{g} + \nu^2 \nabla_3^2 \vec{u}, \tag{B.1}$$

where

$$\begin{aligned}\frac{D}{Dt} &\equiv \frac{\partial}{\partial t} + u\frac{\partial}{\partial x} + v\frac{\partial}{\partial y} + w\frac{\partial}{\partial z} \\ &= \frac{\partial}{\partial t} + \vec{u} \cdot \nabla_3\end{aligned}$$

and Ω the earth rotation vector, $\vec{g}$ the gravitational force, ν the kinematic viscosity and p the pressure. When the hydrostatic approximation is valid B.1 reduces to

$$\begin{aligned}\frac{D\vec{u}_h}{Dt} + \hat{f} \times \vec{u}_h &= -\frac{1}{\rho}\nabla_2 p + \nu^2 \nabla_3^2 \vec{u}_h \\ \frac{\partial p}{\partial z} &= -\rho g,\end{aligned} \tag{B.2}$$

where

$$\hat{f} = 2\vec{k}\Omega_0 sin\phi = f\vec{k}$$

and $\vec{u_h}$ is the horizontal velocity, $\vec{k}$ the vertical unit vector and ϕ the latitude.

Conservation of salinity and heat:

$$\begin{aligned}\frac{\partial S}{\partial t} + \nabla_3 \cdot (\vec{u}S) - \kappa_S \nabla_3^2 S + \Phi^S \\ \frac{\partial T}{\partial t} + \nabla_3 \cdot (\vec{u}T) = \kappa_T \nabla_3^2 S + \Phi^T,\end{aligned} \tag{B.3}$$

where S is the salinity, T the temperature, κ_T the diffusion constant for heat and κ_S for salt.

Conservation of mass:

$$\frac{\partial \rho}{\partial t} + \nabla_3(\rho \vec{u}) = 0, \tag{B.4}$$

where ρ is the density.

Equation of state:

$$\rho = \rho(p, S, T) \tag{B.5}$$

Bijgaand treft U een overzicht aan van recentelijk in deze serie gepubliceerde titels. Een komplete lijst wordt U op verzoek toegezonden. U kunt Uw aanvraag richten aan de KNMI Bibliotheek, Postbus 201, 3730 AE De Bilt (030-206855). Hier kan men U tevens informeren over de verkrijgbaarheid en prijzen van deze publicaties.

89-05 Statistical forecasts of sunshine duration / Li Zhihong and S. Kruizinga.

90-01 The effect of a doubling atmospheric CO2 on the stormtracks in the climate of a general circulation model / P.C. Siegmund.

90-02 Analysis of regional differences of forecasts with the multilayer AMT-model in the Netherlands / E.I.F. de Bruin, Li Tao Guang and Gao Kang.

90-03 Description of the CRAU data-set : Meteosat data, radiosonde data, sea surface temperatures : comparison of Meteosat and Heimann data / S.H. Muller, H. The, W. Kohsiek and W.A.A. Monna.

90-04 A guide to the NEDWAM wave model / G. Burgers.

91-01 A parametrization of the convective atmospheric boundary layer and its application into a global climate model / A.A.M. Holtslag, B.A. Boville and C.-H. Moeng.

91-02 Turbulent exchange coefficients over a Douglas fir forest / F.C. Bosveld.

92-01 Experimental evaluation of an arrival time difference lightning positioning system / H.R.A.Wessels.

92-02 GCM control run of UK Meteorological Office compared with the real climate in the NW European winter / J.J. Beersma.

92-03 The parameterization of vertical turbulent mixing processes in a General Circulation Model of the Tropical Pacific / G. Janssen.

92-04 A scintillation experiment over a forest / W.Kohsiek.

92-05 Grondtemperaturen / P.C.T.van der Hoeven en W.N.Lablans

92-06 Automatic supression of anomalous propagation clutter for noncoherent weather radars / H.R.A. Wessels and J.H. Beekhuis.

93-01 Searching for stationary stable solutions of Euler's equation / R. Salden.

93-02 Modelling daily precipitation as a function of temperature for climatic change impact studies / A.M.G. Klein Tank and T.A. Buishand.

93-03 An analytic conceptual model of extratropical cyclones / L.C. Heijboer.

93-04 A synoptic climatology of convective weather in the Netherlands / Dong Hongnian.

93-05 Conceptual models of severe convective weather in the Netherlands / Dong Hongnian.

94-01 Seismische analyse van aardbevingen in Noord-Nederland : bijdrage aan het multidisciplinaire onderzoek naar de relatie tussen gaswinning en aardbevingen / H.W.Haak en T. de Crook.

94-02 Storm activity over the North Sea and the Netherlands in two climate models compared with observations / J.J. Beersema.

94-03 Atmospheric effects of high-flying subsonic aircraft / W. Fransen.

94-04 Cloud-radiation-hydrological interactions : measuring and modeling / A.J. Feijt, R. van Dorland, A.C.A.P. van Lammeren, E. van Meijgaard en P. Stammes.

94-05 Spectral ultraviolet radiation measurements and correlation with atmospheric parameters / F. Kuik and H. Kelder

95-01 Transformation of precipitation time series for climate change impact studies / A.M.C. Klein Tank and T.A. Buishand

95-02 Internal variability of the ocean generated by a stochastic forcing / M.B.H. van Noordenburg

95-03 Applicability of weakly nonlinear theory for the planetary-scale flow / E.A. Kartashova

95-04 Changes in tropospheric NOx and O3 due to subsonic aircraft emissions / W.M.F. Wauben, P.F.J. van Velthoven and H. Kelder